Comprehensive characterization of propylene carbonate based liquid electrolyte mixtures for sodium-ion cells

Andreas Hofmann[a,*], Zhengqi Wang[a,b], Sebastian Pinto Bautista[c,d], Marcel Weil[c],
Freya Müller[a], Robert Löwe[a], Luca Schneider[a], Ijaz Ul Mohsin[a], Thomas Hanemann[a,b]

[a] Karlsruher Institut für Technologie, Institut für Angewandte Materialien (IAM), Herrmann-von-Helmholtz Platz 1, Eggenstein-Leopoldshafen 76344, Germany
[b] Department of Microsystems Engineering, University of Freiburg, Georges-Köhler-Allee 102, Freiburg D-79110, Germany
[c] Karlsruher Institut für Technologie, Institut für Technikfolgenabschätzung und Systemanalyse (ITAS), Postfach 3640, Karlsruhe 76021, Germany
[d] Helmholtz-Institut Ulm für Elektrochemische Energiespeicherung (HIU), Helmholtzstraße 11, Ulm 89081, Germany

ABSTRACT

In this study, 1 M sodium perchlorate ($NaClO_4$) containing binary electrolytes based on propylene carbonate and X (X = dimethyl carbonate, diethyl carbonate, ethyl methyl carbonate, dipropyl carbonate, ethylene carbonate, 1,2-butylene carbonate, monoglyme, diglyme, tetraglyme, sulfolane) are studied due to their electrochemical and physicochemical properties as well as compatibility with sodium metal. The reactivity towards sodium is compared between mixtures with and without $NaClO_4$ and degradation products are analyzed by gas chromatography. It is shown that $NaClO_4$ plays a crucial role in electrolyte decomposition and gas formation. It could be shown that mixtures of linear and cyclic carbonates form coupling products during storage with Na metal, namely dialkane propane-1,2-diyl dicarbonates, independently of the presence of sodium perchlorate. Additionally, gas analysis of PC electrolyte over Na shows a pronounced formation of CO and propylene oxide during storage if $NaClO_4$ is present in the sample. Overall, the electrolyte "PC+EC+$NaClO_4$" is identified as most favorable system within the examined series with respect to decomposition characteristics (formation of decomposition products) as well as acceptable physicochemical and electrochemical properties, e.g. plating-stripping behavior, cycle tests, conductivity and solubility. A sustainability screening of the electrolyte formulations reveals a high toxic concern in case of glyme-based mixtures as well as sulfolane. From a life cycle perspective, however, glyme-based mixtures have in overall lower environmental footprints.

1. Introduction

Rechargeable batteries are one of the most promising resource for providing electrical energy. Lithium-ion batteries are state of the art today despite some critical issues, such as the availability of battery materials, toxic considerations, and hazards associated with thermal runaway of the cells. Such factors inspire the development of post-lithium technologies, e.g. sodium-ion based batteries [1].

Much efforts are taken to develop novel electrode materials for sodium-ion based cells, however, often the electrolyte is neglected during the optimization process. Thus, up to now, only few solvent systems are described which are mostly following the state-of-the-art Li ion electrolytes composed of carbonate based solvent mixtures [2–8]. An ideal electrolyte for sodium-based batteries has to fulfill similar characteristics compared to Li ion cells, namely low-cost, chemical stability, electrochemical stability, non-toxicity, scalability as well as thermal stability [9,10]. Although effort was made to clarify the interaction between these electrolytes and sodium and/or electrode material by various techniques [10–16], the interactions and reactions on the surface are still not yet understood.

A large number of studies in literature dealt with carbonate-based electrolytes are using ethylene carbonate (EC) as solvent in the electrolyte [1,9,10,17–20]. However, EC exhibits a high melting point of 36 °C, which in itself is unfavorable in the preparation of the electrolytes, but which can also cause EC to crystallize in the electrolyte at low temperatures. In contrast, propylene carbonate (PC) exhibits a melting point of -49 °C due to its molecular structure, and various properties as stability against Na, and key molecular properties ensure that it is often used as a solvent for Na ion batteries [21]. PC is used in Na ion based battery research as a single solvent [3,6,22–32] or in PC+EC binary mixtures due to the favorable properties in half cells [3,27,33–40]. However, the

stability of PC against Na metal is far from being optimal without additives in the electrolyte, as being observed by simply storage sodium metal in PC based electrolytes [32,41]. The identification of improved electrolyte formulations including concentration variations based on known carbonates (EC, PC, butylene carbonate, dimethyl carbonate, diethyl carbonate, ethyl methyl carbonate, dipropyl carbonate, etc.) is rather limited by the large number of potential combinations, especially when additives are additionally used, so that individual combinations are often selected and described in the literature [38]. This is reasonable and can often not be done by any other way. As a result, the effects described have to be considered more or less isolated and consequently limit a deeper understanding of reaction mechanisms over sodium metal and knowledge about electrode-electrolyte interfaces within a class of chemical compounds, in particular to the use of electrode materials, on which the cell behavior also depends to a large extent. Systematic studies on electrolytes are therefore essential to provide correlations, comparative benchmarks and stability (data, statements) in Na based batteries [12,21,31,32].

In sodium-ion batteries, additives are rarely investigated. Most knowledge is provided for 4-fluoro-1,3-dioxolan-2-one (fluoroethylene carbonate, FEC) in terms of sodium stability and increase of cell stability [6,11,16,37–39,42–44] due to the formation of a NaF-rich SEI layer [32]. However, FEC is only favorable in half cells including Na metal, if at all [37]. In full cells, FEC shows mostly a worsening behavior due to overpotential and film formation. The nature of hard carbon (HC) indeed aggravates the investigation of additives as a result of the dependence of the HC surface on the layer composition and the HC material itself. The high reactivity of the sodium surface additionally complicates the investigation of additive effects, since any contamination in the electrolyte from solvent, conducting salt or additive changes the surface of Na. Besides some of the most important additives used for Li ion batteries may be not suitable in case of Na ion based batteries or only in particular formulations (e.g. vinylene carbonate [21,45,46], ethylene sulfite [21], difluoroethylene carbonate [47], etc.). For this reason, the following study largely exposes additive effects in order to address, as a fundamental understanding, the reactivity of the Na interface in the presence of the electrolyte by itself.

NaClO$_4$ is one of the most used conducting salts for Na ion batteries in spite of its oxidizing behavior, especially in academia research. This results from advantageous properties, namely low water sensitivity, high purity, cheap price and good solubility [48], especially in comparison with NaPF$_6$. Nevertheless, versatile functions of the NaClO$_4$ salt need to be further explored, e.g., in terms of stable SEI formation capability and synergistic support in anchoring Na ions in the storage materials. A main disadvantage of sodium perchlorate, especially at larger scales, are safety issues. Nevertheless, for research and development (R&D) investigations, NaClO$_4$ conducting salt offers a trouble-free handling regarding the avoidance of HF in addition to long-term stable electrolyte mixtures in aluminum as well as glass bottles in contrast to NaPF$_6$. It was also observed in the literature that the solubility of NaPF$_6$ in carbonate-based solvents is sometimes inferior, producing an insoluble precipitate. Thus, Bhide was able to detect NaF as a hydrolysis product, making long-term stability of NaPF$_6$-containing electrolytes critical [48]. Other conducting salts as sodium bis(trifluoromethanesulfonyl)imide (NaTFSI) or sodium bis(fluorosulfonyl)imide (NaFSI) are also used and applied in organic as well as aqueous electrolyte systems [49,50].

In the current study, the selected propylene carbonate and NaClO$_4$ containing electrolyte mixtures with selected classes of solvent compounds were investigated with respect to their physicochemical as well as electro-chemical properties. Temperature-dependent density, conductivity and dynamic viscosity data were related to calculated data using the AEM software. The stability

of the electrolyte formulations was analyzed against sodium metal in-depth visually, and liquid as well as gaseous products were analyzed by gas chromatography in detail. Electrochemical measurements were performed to quantify surface effects and cell performance.

2. Reagents and methods

2.1. Chemicals and materials

Propylene carbonate (PC, 99.7%, anhydrous, ACROS Organics), dimethyl carbonate (DMC, ≥99%, anhydrous, Sigma Aldrich), diethyl carbonate (DEC, 99%, anhydrous, ACROS Organics), ethyl methyl carbonate (EMC, ≥99%, Merck Chemicals), dipropyl carbonate (DPrC, ≥98%, BOC Sciences), ethylene carbonate (EC, Ultrapure®, HUNTSMAN), 1,2-butylene carbonate (12BC, >98%, Tokyo Chemical Industry), 1,2-dimethoxy ethane (G1, monoglyme, ≥99% ultra-dry, ACROS Organics), Di(2-methoxyethyl) ether (G2, diglyme, ≥99% ultra-try, ACROS Organics), Bis[2-(2-methoxyethoxy)ethyl] ether (G4, tetraglyme, 99%, ultra-pure, ACROS Organics) and sulfolane (SL, 99%, Sigma Aldrich) were dried over molecular sieve for 2 days before usage. Pentane (≥99%, anhydrous, Sigma Aldrich) was dried over molecular sieve or by immersing sacrificial Na flakes. Sodium perchlorate (NaClO$_4$, anhydrous, 98.0–100.0%, Alfa Aesar) was dried at 105 °C for 48 h under vacuum (vacuum oven inside glove box). Glass vials and tips for pipettes were heated at 75 °C at 48 h in vacuum. Sodium (cubes, stored under mineral oil, 99.9% trace metals basis, Sigma Aldrich). Preparation of sodium pieces: Cutting off the surface oxidation film of a sodium cube with a stainless steel scalpel and then cutting into thin slice at the fresh side of the sodium cube; sandwiching the slice in between plastic foil and then extending the slice into homogeneous thin foil by using a hydraulic press; removing the surface oil on the sodium foil with filter paper and pentane; cutting the foil into the desirably sized Na pieces for further usage). Hard carbon (HC, $d = 16$ mm) and Cu (d = 12 mm) were punched out and dried at 95 °C for 48 h. Handling of all chemicals and materials was done in an Ar filled glove box from Braun (O$_2$ and H$_2$O concentrations were below 0.5 ppm).

2.2. Solubility

The solubility data were received by observation of the salt-dissolution in every single solvent liquid. Briefly, 100 mg of salt was weighted in a vial, in which a controlled small amount of solvent (15–100 mg, dependent on the residual salt solid) was added, until the basic salt was totally dissolved. To obtain a very nearly saturated salt-in-solvent solution, a certain amount of salt (25 mg) was added again into the fully dissolved salt-solution formed at the last step, and then the controlled amount of solvent was furtherly added, to dissolve the precipitated salt caused by repeated salt addition. By the repeated procedures the nearly solubility limit could be calculated. The operation was done at 25 °C and a stable dissolved status of a liquid was confirmed, by hand-shaking, slight tapping, and observation over days, to ensure no more nucleation of crystals formed.

2.3. Conductivity

The ionic conductivity of the electrolyte mixtures was measured by standard complex impedance method with a Zahner Zennium IM6 electrochemical workstation in the frequency range from 50 kHz to 1 MHz. The closed cell from RHD instruments was filled with 0.85 ml of solution for the measurement. In the phase minimum ($\approx 0°$), the absolute value of complex impedance $|\vec{z}|$ was used for calculating the specific conductivity κ according to

$\kappa = C/|\vec{z}|$ with the cell constant C. The cell constant C was obtained by measuring standard KCl-solution (1.413 mS cm^{-1} at 25 °C, Hanna instruments, HI 70031). The value of the internal resistance, mentioned above, was extracted from $|\vec{z}|$ of the Bode plot at the minimum of phase angle ($\approx 0°$).

2.4. Viscosity

The dynamic viscosity was measured with a Malvern Gemini HR Nano rotational rheometer by using 40/1° cone geometry with a sample filling gap of 30 μm. A solvent-evaporation-protection cover in air was used during measuring. The measurements were performed at the temperature range of 15–70 °C and a series of increased shear rate (5–200 s^{-1}) at each temperature.

2.5. Density

The density values of the electrolyte mixtures were measured with Anton Paar DMA 4500M at the temperature range between 20 and 60 °C.

2.6. Cyclic voltammetry

The cyclovoltammograms were measured with a Zahner XPOT potentiostat (software: PPSeries, Potentiostat XPot Zahnerelektrik 6.4). The cathodic scans were measured in a Swagelok-type cell with bare copper foil electrode (Ø = 12 mm) as working electrode and Na as counterpart (Ø = 12 mm); the cathodic potential was applied between 2 and 0 V vs. Na/Na$^+$ for three cycles (the first cathodic scan began from 3 V vs. Na/Na$^+$, close to the open-circuit-voltage) and subsequently between 2 and -0.5 V for further 2 cycles. The anodic scans were applied between 3 and 6.5 V vs. Na/Na$^+$ in the 2-electrode configuration of a three-electrode cell (EL-Cell GmbH, Hamburg, Germany) with Na (Ø = 16 mm) and platinum (Ø = 18 mm) as reference/counter and working electrode, respectively and in between a separator fiber (Ø = 19 mm, GF/B, Whatman®) soaked with 175 µl electrolyte. The scan speed was 2 mV•s^{-1} for all tests.

2.7. Electrolyte stability

Cutted sodium plates (approximately 0.1 cm^2) were immersed into electrolyte mixtures and the mixtures were stored inside of the glovebox at 25 °C. After 20 days, the visible observation was documented. 15 µl liquid was extracted from every mixture to prepare the sample for gas chromatography analysis (after 4 month of storage).

2.8. Gas chromatography

Gas chromatography (GC) experiments were performed as described in literature [51] in detail. Briefly, a Clarus 690 GC from PerkinElmer Inc. (Waltham, USA) equipped with an autosampler, a flame ionization detector (FID) and a MS detector (SQ 8T) was used for the measurement and Turbomass 6.1.2 and TotalChrom 6.3.4 software packages were used for data acquisition as well as data analysis. Following parameters were used during the measurement: *Gas*: He 6.0 (Air Liquide), H$_2$ gas from hydrogen generator PG+160 (Vici DBS), Air (Air Liquide); *Column*: Optima 5MS, 30 m length x 0.25 mm interior diameter, 0.5 µm film thickness; *Parameters during injection*: split flow of 20 ml/min, inlet temperature of 250 °C, 0.5 µl injection volume, 175 kPa initial pressure, pressure controlled mode, oven temperature 40 °C; *Oven and pressure parameters*: 40 °C for 1.5 min, heating at 20 °C/min up to 320 °C. Pressure starting from 175 kPa for 2 min, increase at 7.8 kPa/min up to 300 kPa; *MS setup*: filament voltage of 70 kV,

ion source temperature of 200 °C, MS transfer line temperature of 200 °C; *FID setup*: 450 ml/min for synthetic air, 45 ml/min for hydrogen gas FID temperature of 280 °C. The gas flow was split up by a SilFlow^{TM} GC Capillary Column 3-port Splitter after the separation column in order to detect the signals in the MS as well as in the FID. The FID was used for quantification whereas the MS was used for identification. Therefore, the MS was used in the scan mode with a scanned range from 33 u to 350 u and an event time of 0.3 s (interscan delay of 0.02 s). The signals from the FID were used for determining the peak area. All samples (electrolytes, mixtures) were compared and corrected against pure dilution solvent as well as pure electrolyte solvent. Impurities in the electrolyte solvents were analyzed when possible, based on NIST search (EI fragmentation match) as well as measuring the pure substance.

The formation of gas was tested in a PAT-Cell-Press (EL Cell) where the spring in the upper case was removed and a cup with electrolyte and sodium was placed in the lower case. After closing, the pressure was monitored. The gas was extracted with a syringe including a syringe lock to prevent atmospheric gas to penetrate into the syringe. The gas was injected into the GC device and qualitatively analyzed.

2.9. Cell testing

Full-cells of hard carbon|Na$_{0.7}$MnO$_2$ (Ø = 16 mm) were assembled in standard 2032-type coin cell in an Ar-filled glove box with moisture and O$_2$ content below 0.5 ppm. A glass fiber separator (Ø = 17 mm, QMA, Whatman®) wetted with a 110 µl electrolyte mixture was used. The electrodes and separators were dried under vacuum (110 °C, 24 h) prior assembling within a cell. The theoretical area capacity of the electrode plates was 2.2 mAh cm^{-2} for hard carbon and 0.5 mAh cm^{-2} for sodium manganese oxide. Galvanostatic charge-discharge cycling were carried out with the cell cycler LICCY (developed by KIT, Institute of Data Processing and Electronics). Cell tests were firstly conducted at a series of continually increased current rates (C-rate of charging/discharging as following: 0.1C/0.1C, 0.2C/0.2C, 0.5C/0.5C, 0.5C/1C, 0.5C/1.5C, 0.5C/5C, 0.5C/7.5C, 0.5C/10C for 1–3 cycles), and subsequently the cells were cycled at the reduced rate (0.2C/0.2C for 2 cycles, 0.5C/1C for 100 cycles and 0.2C/0.2C for 2 cycles). The C-rate applied was based on the capacity of the cathode materials used.

2.10. Electrolyte simulation with AEM software

The advanced electrolyte model (AEM) approach to calculate viscosity, density, conductivity, etc. values have been published and result from various chemical-physical terms derived for multi-member electrolytes [52–54]. We used the software package from INL to calculate these values. The Advanced Electrolyte Model software may be available for licensing from Idaho National Laboratory. Contact td@inl.gov for more information.

2.11. Thermogravimetry analysis

The thermogravimetry analysis was done with the device STA 449 F3 from Netzsch. 47.9 mg of PC+EC+1 M NaClO$_4$ electrolyte was put in an Al$_2$O$_3$ crucible (open) and measured under an dry air atmosphere between 25 °C and 800 °C. The temperature ramp was set to 10 K•min^{-1}. In parallel, the DSC curve was recorded.

2.12. Sustainability

2.12.1. Hazard traffic light (HTL)

This qualitative method is a color-code of potential hazards for different substances first presented by Rodriguez García et al. [55]. It is based on the hazard statements described in the regulation

of the European Parliament on classification, labeling and packaging and as registered by the European Chemicals Agency – ECHA (www.echa.eu) for each material [56]. A total number of 62 hazard statements grouped in 28 hazard classes are defined, each with a code, pictogram and signal words such as 'danger', 'warning' or no hazard word. An additional distinction between physical, health and environmental hazard is also taken into account. It is often the task of the producers and suppliers to classify their products following the previous guidelines, but for some specific substances a harmonization is done at the EU level, when the perceived hazards are of major concern. Ultimately, a color is assigned to each hazard statement based on the respective signal word that it has received, which allows for a visual distinction of the potential hazardousness of a material. Red color will be assigned to hazards labelled as 'danger', whereas yellow will be used for those presented as 'warning'. Statements without a hazard word are colored in gray.

2.12.2. Hazard level (HL)

Initially presented by the German Environmental Agency (UBA) [57], this quantitative methodology uses the hazard statements previously described for the HTL. A ranking of each hazard is made based on the maximum tonnage of a substance that can be stored without implementing specific safety measures, also referred as Major-accident Prevention Policies (MAPP). This tonnage is described by the Lower Tier (*LT*) values presented in the 2012/18/EU Directive of potential hazardousness of materials [58]. Ultimately, only the minimum of all the LT of a material is used and the inverse value is calculated to express its hazard score more intuitively. The method was further developed by Rodriguez-Garcia et al. [55], who suggested that including all the LT for the different hazards of a material would provide a more comprehensive picture of its hazardousness, as the original method reduces a material to a single hazard. The total HL of a substance can then be calculated by using the following Eq. (1):

$$HL = \sum_{i}^{n} \frac{1}{LT_i} \qquad (1)$$

2.12.3. Life cycle assessment (LCA)

This method consists in an evaluation of the different environmental impacts of a product along the different stages of its life cycle, such as raw material acquisition, manufacturing, use and final disposal, and follows the guidelines described by the ISO Standards 14040/14044 [59,60]. Such impacts are associated to material and energy flows as well as waste and other emissions produced in each of these stages. For the specific case, a cradle-to-gate analysis has been performed, meaning that the impacts are estimated only until the final stage of electrolyte production. A functional unit of 1 L of electrolyte mixture has been chosen. The analysis was performed using the ReCiPe midpoint 2016 impact assessment methodology, which describes a set of 18 impact categories each with a specific reference unit [61]. Additionally, a calculation of the cumulative energy demand (CED) can be found in Table DB-9 (Data in Brief). The CED describes the total energy consumption from non-renewable sources until the final step of production of the mixtures. The synthesis of precursor materials has been modeled with data from published patents and literature sources as well as the commercial life cycle inventory (LCI) database Ecoinvent 3.7.1. The assessment was conducted using the software OpenLCA v1.10 [62–68].

3. Results and discussion

3.1. Solubility of NaClO₄ in the solvents and thermal properties of the electrolytes

In this study, electrolyte formulations based on PC and $NaClO_4$ were investigated, namely binary mixtures of PC and commonly used battery solvents. The selection of the solvents was motivated on the basis of preliminary studies and on the widespread use of these substance classes in terms of comparability and comprehensive overview and inspired to obtain an overview about these solvents for Na ion batteries. Sodium perchlorate was chosen based on its widespread use in Na-based battery systems, its low reactivity and low hydrolysis sensitivity compared to $NaPF_6$ salt. Additionally, the electrochemical stability against Al is much better than for the NaTFSI salt. Within this study, $NaClO_4$ was selected despite its pronounced tendency to oxidation, in particular to exclude side reactions not causally related to the Na contact during the preparation of the electrolytes due to decomposition with water traces, HF, POF_3, and others [49]. Table 1 summarizes the properties of pure solvents as well as the solubility of sodium perchlorate in these solvents. With exception of EC and SL, all solvents are in liquid state at 25 °C ($p = 1$ atm), and exhibit boiling points between 90 and 285 °C ($p = 1$ atm), which make them suitable as battery solvents. All electrolyte formulations with PC remain liquid down to 0 °C. PC, EC, 12BC, G4 as well as SL exhibit high flash point values of >100 °C, which further improve the electrolyte safety in terms of flammability and fire risk. Table 2 summarizes the properties of the binary mixtures.

It is seen that all mixtures remain liquid and completely soluble down to 0 °C. The composition of the 1:1 mol/mol binary mixtures is provided also in wt./wt. ratios. Molar ratios were used to ensure the comparability of the number of molecules from each species in each mixture. The solubility of $NaClO_4$ in linear carbonates (DMC, DEC, EMC and DPrC) is relatively low, but 1:1 molar mixtures with PC ensure a solubility up to 1 M $NaClO_4$ up to C_2 chain length of the linear carbonate. In case of DPrC (C_3 chain length) a 3:1 molar ratio (PC:DPrC) is necessary to ensure full dissolution of the salt. It can be seen that due to the large molecular masses of the larger glyme derivatives, the wt. content of PC increases, (e.g. in PC+G4 mixture). Other wt. ratios are almost balanced.

3.2. Density, conductivity and viscosity values of the electrolytes

Temperature dependent conductivity and viscosity data of the mixtures were measured and calculated using the AEM model. The values for all systems are depicted in Fig. 1 as an overview at 25 °C. Detailed values of all measurements and calculated data are provided in the Data in Brief article (Tables DB-1 to DB-5). It is observed that the results based on the AEM model exhibit good agreement to the experimental values for many of the electrolytes in spite of a complex electrolyte system. Two solvents (DPrC, 12BC) are not listed in the software database, thus these mixtures could not be calculated accordingly. The data reveal that the calculation of these properties is a meaningful possibility to provide a first estimation of the quantity of these values in case of unknown electrolyte formulations and to predict the temperature dependency of these physicochemical characteristics.

The density values of the electrolytes describe the electrolyte mass per volume and thereby directly influence the mass-related energy density. However, density values are of course only one factor among several, with the chemical and electrochemical suitability of an electrolyte obviously taking priority. High density values are found for cyclic carbonates and PC+SL mixture, namely PC+EC > PC+SL > PC > PC+12BC. In contrast, glyme containing mixtures exhibit smaller density values which favor the realization of higher energy densities. Excellent matching is received for the density values with deviation less than 2% between experimental and calculated data, enabling the corresponding density values to be predicted well with the AEM software. Known data in the literature (e.g. PC+EC+1M $NaClO_4$) show a precise matching of the density values, e.g. 1.3297 g•cm⁻³ (this work) vs. 1.33 g•cm⁻³ in Ref. [40].

Table 1
Solubility data of NaClO$_4$ in pure solvents. The flash point (*fp.*), melting point (T_{mp}), the boiling point (T_{bp}) of pure solvent and the dielectric constant (ε_r) is provided. NA = not available.

	solubility g NaClO$_4$/ 1 kg solvent	M g ·mol^{-1}	*fp.* ° C	T_{mp} ° C	T_{bp} °C	ε_r (T / °C) at 1 kHz
PC	228	102.09	132	-55	240–243	66.4 (20)
DMC	45	90.08	18	2–4	90	3,8 (20)
DEC	<35	118.13	25	-43	126–128	2,8 (20)
EMC	<35	104.10	23	-14.5	107	3.0 (20)
DPrC	<35	146.18	55	-41	167–168	NA
EC	>200 (60 °C)	88.06	143	35–37	238–244	95.3 (25)
12BC	131–136	116.12	135	-45	281	57.5 (20)
G1	500	90.12	5	-69	84–86	7.1 (25)
G2	502	134.18	57	-64	162	7.4 (25)
G4	262	222.28	136	-30	275–276	7.8 (25)
SL	106 (60 °C)	120.17	165	27–28	285	NA
NaClO$_4$	–	122.44		468	482[a]	–

[a] decomposition.

Table 2
Experimental values of solubility, density (*d*), melting point (T_{mp}), conductivity (κ) and viscosity data (η) of the PC+X electrolytes at T = 25 °C.

| solvent mix 1:1 (mol)	salt	d (25 °C) g·cm^{-3}	liquid/soluble 25 °C	liquid/soluble 0 °C	liquid/soluble - 30 °C	T_{mp}(DSC) °C	wt./wt. solvent	κ (25 °C) mS•cm^{-1}	η (25 °C) mPa•s
PC	1 M NaClO$_4$	1.2616	+	+	+	-54	100	5.8	7.3
PC+DMC	1 M NaClO$_4$	1.2105	+	+	+	-23	53.1/46.9	7.4	4.1
PC+DEC	1 M NaClO$_4$	1.1439	+	+	+	-48	46.4/53.6	4.3	4.1
PC+EMC	1 M NaClO$_4$	1.1741	+	+	+	-50	49.5/50.5	5.6	3.9
PC+DPrC[a]	1 M NaClO$_4$	1.1726	+	+	+	-52	67.7/32.3	3.6	6.4
PC+EC	1 M NaClO$_4$	1.3243	+	+	+	-4	53.7/46.3	7.1	6.8
PC+12BC	1 M NaClO$_4$	1.2353	+	+	+	-48	46.8/53.2	4.2	8.3
PC+G1	1 M NaClO$_4$	1.1082	+	+	+	-46	53.1/46.9	10.0	3.4
PC+G2	1 M NaClO$_4$	1.1241	+	+	+	-52	43.2/56.8	7.9	4.3
PC+G4	1 M NaClO$_4$	1.1363	+	+	+	-45	31.5/68.5	3.2	10.9
PC+SL	1 M NaClO$_4$	1.2984	+	+	–	18	45.9/54.1	3.2	14.7

[a] PC/DPrC = 3:1 (mol/mol).
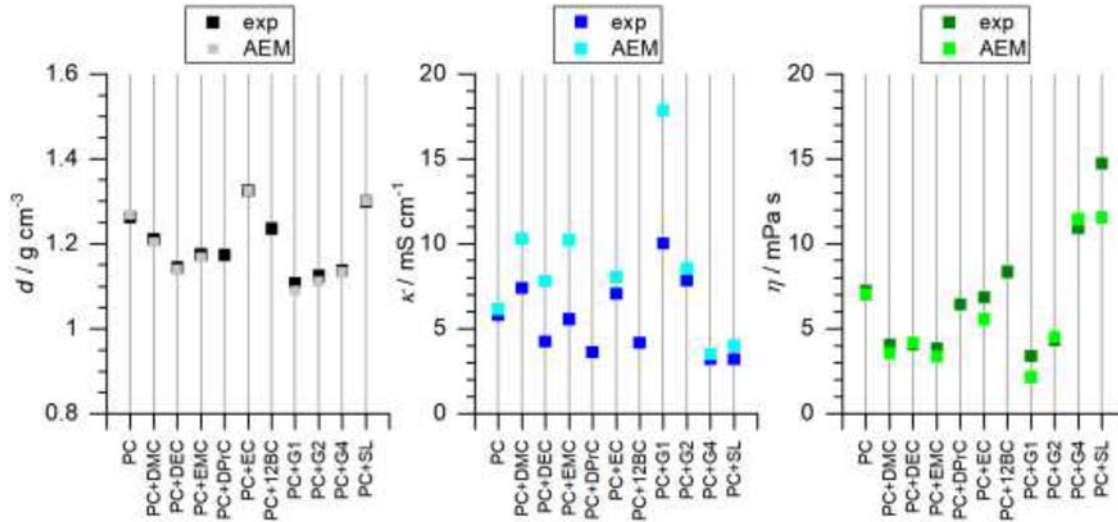
Fig. 1. Density (*d*), conductivity (κ) and viscosity (η) values of the electrolyte mixtures at T = 25 °C. Experimental values (exp) are compared to calculated values (ANL) with AEM approach.

The conductivity data of the electrolytes vary between 3 and 10 mS•cm^{-1} and the viscosity data are in a range between 3 and 15 mPa•s at T = 25 °C. These values are common for battery electrolytes and ensure a suitable transport of Na$^+$ ions, which is necessary for battery use. PC+G1 electrolyte exhibits the highest conductivity values and, accordingly, the lowest viscosity value at 25 °C from all mixture, whereas PC+G4 and PC+SL based electrolytes exhibit the worst characteristics (κ, η) in terms of battery electrolyte use. The characteristics correlate well with the molecular structure of the pure compounds, e.g. the graded chain length from G1 to G4, which result in an increase of viscosity data and correspondingly a decrease of conductivity data. Such trends are also found from short to longer linear carbonates (DMC to DPrC) accordingly. Interestingly, the conductivity is higher for 1 M NaClO$_4$ electrolytes with the solvent mixture PC+EC than for PC+DEC, PC+EMC and PC+DPrC, reaching almost PC+DMC values. This is remarkable due to the high boiling points of both solvents PC and EC. Ponrouch et al. provides comparable values
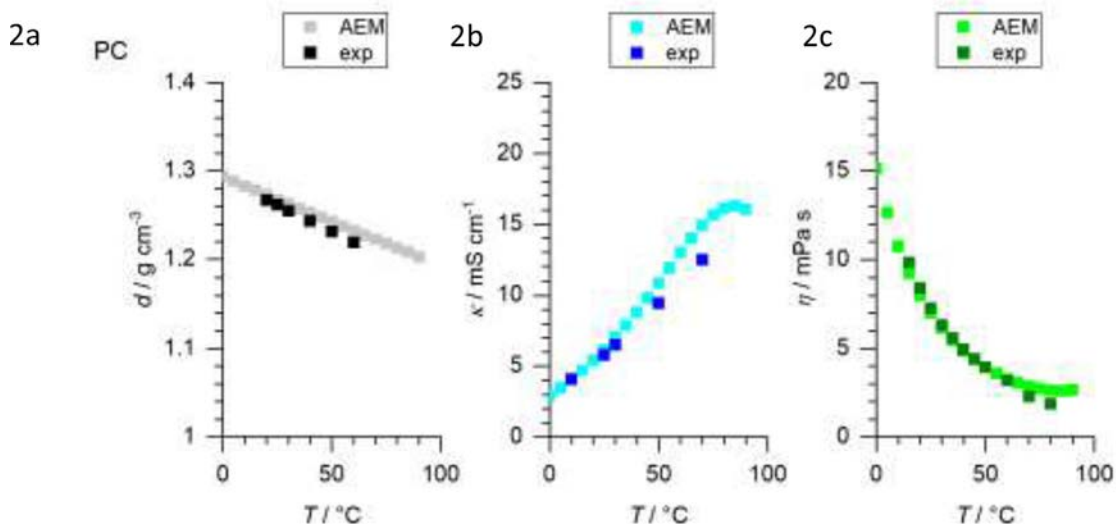
Fig. 2. Temperature-dependent density (2a), conductivity (2b) and viscosity (2c) data of 1 M NaClO$_4$ in PC.
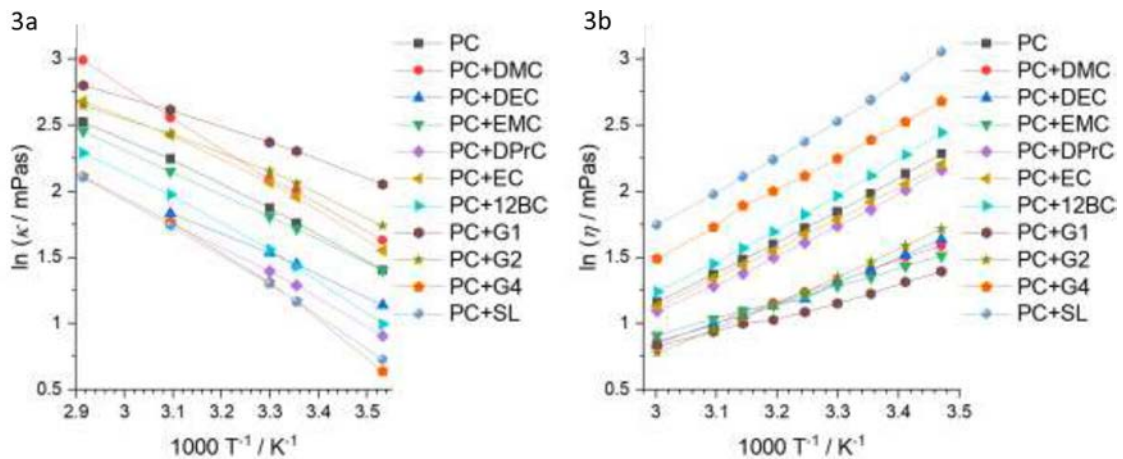

Fig. 3. Temperature dependency of conductivity (3a) and viscosity (3b) values from all electrolyte mixtures (PC+X+NaClO$_4$).

for conductivity and viscosity data, namely $\kappa = 6.4$ mS•cm^{-1} and $\eta = 6.8$ mPa•s (PC+1 M NaClO$_4$, 20 °C) [3]. Similarly, Benchaker at al. provided comparable results on the system EC+PC+1 M NaClO$_4$, namely $\kappa = 7.57$ mS•cm^{-1} and $\eta = 6.27$ mPa•s at 20 °C [40]. The temperature-dependent plot for electrolyte PC+NaClO$_4$ is exemplarily shown in Fig. 2 and the temperature dependent data of all other electrolytes including the AEM calculated values is shown in the Data in Brief article (Figs. DB-1 to DB-10) for a detailed view. The temperature-dependent viscosity and conductivity data exhibits the well-known behavior in terms of increase of the conductivity and strong decrease of the viscosity (both with increasing temperature). It is remarkable that the calculated AEM results show a significant flattening of the increase in conductivity between 75 and 100 °C, but, in general, the calculated data match the experimental data within the full temperature range magnificently. Arrhenius plots of all experimental conductivity and viscosity data (experimental values) as an overview are shown in Fig. 3 within a temperature range between 10 and 70 °C. Almost linear plots are received for the viscosity data within the temperature range and for most of the conductivity data. If the conductivity values are compared directly at 50 °C and 25 °C, it is found that they differ by a factor of 1.4–1.8 (factor of conductivity enhancement), whereas electrolyte PC+G4 is most pronounced (factor 1.83). The decrease in the viscosity values is for all mixtures in the same or-

der of magnitude, namely between 0.5 and 0.7, based on the experimental values at 25 °C and 50 °C.

Salt diffusion coefficients were calculated within the AEM approach and listed at $T = 25$ °C in Table DB-2a (Data in Brief). High diffusion constants are obtained for PC+G1 ($D = 2.8•10^{-10}$ m^{2}s^{-1}), PC+EMC ($D = 1.7•10^{-10}$ m^{2}s^{-1}) and PC+DMC ($D = 1.6•10^{-10}$ m^{2}s^{-1}), whereas mixtures from PC+G4 ($D = 0.54•10^{-10}$ m^{2}s^{-1}), PC+SL ($D = 0.58•10^{-10}$ m^{2}s^{-1}) and pure PC ($D = 0.87•10^{-10}$ m^{2}s^{-1}) electrolyte exhibit significant smaller salt diffusion coefficients. This finding is in accordance with flow activation characteristics of the electrolytes. The experimental flow activation energy can be calculated according to the well-known Arrhenius Eq. (2) with the ideal gas constant R and the temperature T in Kelvin.

$$\ln \eta = \frac{1}{T} \cdot \frac{\Delta E_A}{R} + \ln \eta_0 \tag{2}$$

Often, the linear behavior is only given in a limited temperature range, thus the flow activation energy is dependent on this temperature. It is observed that the diffusion coefficients correlate well with the flow activation energies in such a way that high activation energies lead to low diffusion coefficients. This is also consistent with the intermolecular view in solution that ions exposed to a higher mobility barrier have poorer diffusion coefficients. All

Table 3
Selected samples of time-dependent aging of sodium/electrolyte mixtures. All data are shown in the Data in Brief (Table DB-6).

solvent mix	mixture without NaClO$_4$		mixture with NaClO$_4$	
1:1 (mol)	without Na	over Na after 20d	without Na	over Na after 20 d
PC				
PC+DMC				
PC+EC				
PC+G1				
PC+SL				

Arrhenius flow activation energy data ΔE_A cover a range between 10.6 and 23.1 kJ•mol^{-1}. Trends are seen within related groups of electrolytes, e.g. PC+DPrC > PC+DEC > PC+DMC > PC+EMC and PC+G4 > PC+G2 > PC+G1 (ΔE_A values is descending order). The graduation between EMC and DMC, which seems surprising at first view, can be explained by the fact that the inter-molecular inter-action leads to a disorder in the case of an asymmetric molecular structure (EMC), which favors the flow properties compared to a symmetric molecular structure (DMC). Electrolytes, which are composed of cyclic carbonates, exhibit E_A values in a narrow range of sizes, namely 19–21.5 kJ•mol^{-1}.

3.3. Visible formation of impurities between electrolyte and sodium metal

It was investigated how the mixtures behave, when they come in contact with sodium metal and when NaClO$_4$ salt was added or not. Selected results after 20 d of storage (each substance class) are shown in Table 3 and all data are presented in the Data in Brief article (Table DB-6). It is clearly apparent that even after short time of storage at room temperature, the mixtures begin to form visible products, especially in case of sodium perchlorate presence. Pure PC shows almost no reaction after 20 d with the presence of NaClO$_4$ (slightly yellowish color), whereas Pan et al. described a significant aging already after 7 days, which might be an effect of the solvent purity (99.7% anhydrous vs. 99%) and different salt concentrations (1.0M vs. 0.8M) [32]. It is noticeable that the mixtures of "PC+linear carbonate" show extensive decomposition, when NaClO$_4$ is present, which is also in good accordance to the results from Pan et al. [32], but almost no visible decomposition is seen without the salt. In contrast, the "PC+glyme" mixtures indicate strong formation of decomposition products without salt, but much less visible decomposition is found with NaClO$_4$ salt. These findings are congruent within the class of linear carbonates (DMC, DEC, EMC, DPrC) as well as glymes (G1, G2, G4), but a decreasing order of visible decomposition is observed from short to longer

chain length (highest content of decomposition in case of PC/DMC and PC/G1: DMC>EMC>DEC>DPrC and G1>G2>G4). Most of the colored products in both formulations (PC+carbonates, PC+glymes) are solid ones (salts, oligomers, polymers), as filtration (syringe filter, 0.2 μm) resulted in pale yellowish colored solutions in all cases. It should be mentioned that decomposition products may be present even if no color change is observed. On the other hand, however, colored samples clearly indicate the instability between Na surface and electrolyte. It is assumed that NaClO$_4$ can promote or inhibit reaction pathways through complexation of ions, forming different Na surfaces (e.g. including Na-Cl) and interaction with solvents and intermediates, dependent on the solvent composition, which influences the decomposition and electrolyte reactivity significantly. The high stability of PC and PC+EC electrolytes is in accordance to electrochemical data from Ponrouch et al. revealing a high stability for short periods of time [3].

The color of the sodium surface shifts to an orange color when glymes are present (with and without salt), thus a reaction on the surface takes place additionally leading to a surface film on sodium metal. Pure PC as well as PC+EC mixtures exhibit almost no visible formation of products, whereas PC+12BC and PC+SL show a yellow color when sodium perchlorate is available. In repeated experiments it is found that the reaction rate regarding decomposition may vary but it was observed for all samples. This might be due to the highly reactive sodium surface which is difficult to control even under protective atmosphere. The reactivity of sodium towards organic mixtures is similar to that described by Pfeiffer et al. and Pan et al. for selected EC/DMC and PC based electrolytes and demonstrates the difficulty to use Na as electrode material, e.g. counter as well as reference electrode, or to study stripping/plating experiments [32,41].

3.4. Gas chromatography analysis of the electrolytes

Gas chromatography measurements of pure compounds, pure mixtures, salt-free mixtures as well as electrolytes including

Table 4
Results of pure solvents with gas chromatography including EI fragmentation. Measurement of pure compounds.

solvent		retention time (FID) [min, Peak maximum]	retention time (MS) [min, onset]	RI[a]	RI[b] NIST	mass fragmentation m/z in descending intensity order				
Propylene carbonate	PC	6.66	6.67	985	931	57	43	87	44	58
Dimethyl carbonate	DMC	2.91	2.99	615	620	45	59	90	62	60
Diethyl carbonate	DEC	4.56	4.64	781	767	45	91	63	43	59
Ethyl methyl carbonate	EMC	3.70	3.78	697	(662)	45	77	59	44	43
Dipropyl carbonate	DPrC	6.49	6.57	975	(960)	43	63	59	41	104
Ethylene carbonate	EC	6.56	6.43	960	(814)	88	43	44	58	42
1,2-Butylene carbonate	12BC	7.58	7.56	1085	–	43	87	42	44	86
1,2-Dimethoxyethane	G1	3.22	3.30	647	645	45	60	90	58	43
Bis(2-methoxyethyl) ether	G2	6.20	6.27	943	951	59	58	45	89	43
Tetraethylene glycol dimethyl ether	G4	10.54	10.62	1497	(1395)	59	58	103	45	87
Sulfolane	SL	8.71	8.69	1225	–	41	56	55	120	39

[a] RI values are provided based on n-alkanes according to the method described in the manuscript, namely Eq. (1).

[b] NIST based RI values for capillary columns (experimental) are provided for comparison. Values in brackets are estimated non-polar retention index values.

$NaClO_4$ were investigated to gain a more detailed insight about the formation of soluble, non-polymeric decomposition products in presence of sodium metal. In contrast, the composition of the surface of Na metal was not taken into account for this work. Table 4 summarizes the parameters of the pure solvents, namely retention time, retention index and EI fragmentation, whereas Tables DB-7 and DB-8 (Data in Brief) list selected impurities as well as decomposition products. The linear retention indices $I_L(S)$ (non-isothermal Kovats retention indices) were calculated according to the well-known Eq. (3) of Van den Dool and Kratz, where t_n and t_N are retention times of the reference n-alkanes (ideal: eluting directly before and after the compound), i is the difference in length of both n-alkanes (ideal: $i = N - n = 1$), and t_c is the retention time of the proposed compound [69,70].

$$I_L(S) = 100n + 100i\left(\frac{t_C - t_n}{t_N - t_n}\right) \quad (3)$$

Unfortunately, such values are listed very rarely in literature in the field of battery research although they allow a direct comparison of the detected species among different instrument setups. Thus, these data are valuable rather than mentioning retention times or displaying chromatograms only. All linear retention indices $I_L(S)$ listed in the manuscript are determined based on capillary column: Optima 5MS, length of 30 m, inner diameter of 0.25 mm, film thickness of 0.50 μm, T ramp (see experimental conditions), column split and MS onset detection of all peaks (also all n-alkanes). The onset time was used due to the fact, that the peak maximum sometimes varies in dependence of the concentration in the sample, especially at high concentrations if the peak form is not ideal (fronting and/or tailing due to worse substance-to-column interaction or high concentration). Exemplarily, tailing was observed for relative polar compounds, such as alcohols and fronting was observed in case of the solvent signals. In this case, a compromise had to be found between column loading limits of the electrolyte solvents and the most sensitive detection of impurities. All n-alkanes are listed in Table DB-7 (Data in Brief). In Fig. 4, exemplarily, the chromatograms are shown for mixtures containing PC and EC. Chromatograms of all other mixtures as well as pure PC solvent are shown in the Data in Brief article (Figs. DB-12 to DB-21). It is found that solvents which are not available in battery grade, contain impurities, which may be relevant to the cell and/or sodium reactivity, e.g. alcohols (found in 12BC and G4). Ether impurities are detected in DPrC, G1, G2 and G4. In glyme-based solvents, butylated hydroxytoluene is contained as stabilizer. It should be noted that relatively large amounts of DMC and DEC are found in EMC, which is dependent on the EMC supplier and/or drying of the substance (e.g. molecular sieve).

In Fig. 4, the formation of soluble and non-polymeric decomposition products is observed for the salt mixture (PC+EC+1

M $NaClO_4$ with Na metal), namely propylene oxide (FID peak max: 2.13; RI = 485), ethylene glycol (FID peak max: 3.56 min; RI = 694), 1,2-propanediol (FID peak max: 4.04 min; RI = 734) and diglyme (FID peak max: 6.18 min; RI = 945). These compounds are confirmed by the retention time of pure substance, RI comparison with NIST database as well as their EI fragmentation. In contrast, no decomposition products are observed in the $NaClO_4$ free PC+EC electrolyte over Na. This indicates a strong influence of $NaClO_4$ either on the Na surface by forming a different interface layer or the complexation of carbonate molecules in solution.

Selected reaction products are determined based on the fragmentation, NIST comparison and/or retention (retention index) of the determined compound (Table DB-8, Data in Brief), however, a detailed analysis of all decomposition products of all mixtures was not possible. In Fig. 5, an overview about all mixtures is provided by showing the total sum of all decomposition products found in the Na/electrolyte mixture with FID detector related to the total solvent amount (peak area of PC+X). Due to the fact that the area cannot directly used for a quantification, this is an attempt to depict the variety of different products formed by simply storage the Na/electrolyte sample and to provide a rough estimation about the amounts of composition. PC+EMC electrolyte contains a large extent of DMC as well as DEC (Data in Brief, Fig. DB-22) which formed during storage, but which was neglected in Fig. 5 for an overall comparison. It can be seen that in case of salt samples the formation of new compounds increases significantly for PC+carbonate as well as PC+SL mixtures, whereas PC+glyme electrolytes exhibit a reduced reactivity. This is in good accordance with the visible decomposition (Section 3.3). It can be observed that PC+$NaClO_4$ electrolyte in contact with Na metal forms a variety of decomposition products, namely propylene oxide (FID peak max: 2.11 min; RI = 485), 1,2-propanediol (FID peak max: 4.04 min; RI = 734) and diisopropyl carbonate (FID peak max: 5.43 min; RI = 868). These products were found in almost all mixtures due to their PC content.

It is observed that for each electrolyte mixture mainly a few compounds contribute to a large extent to the decomposition products. In case of "PC+linear carbonate" mixtures these compounds, which correspond to larger area bars in Fig. 5, were investigated in a more detailed view. It is observed that solvent mixtures based on linear and cyclic carbonates in contact with sodium metal (with and without $NaClO_4$) exhibit the formation of compounds which show similarities in retention times as well as mass fragmentation compared to the well-known dicarboxylates formed by ethylene carbonate and linear dialkyl carbonates [2,71–76]. The chromatograms as well as EI fragmentation of these compounds (proposed structures: A - D) are shown in Fig. 6 in more detail and the proposed structures are depicted in Fig. 7. Characteristic mass fragmentations are m/z = 44, 45, 58, 59, 73 and 103, 104. These
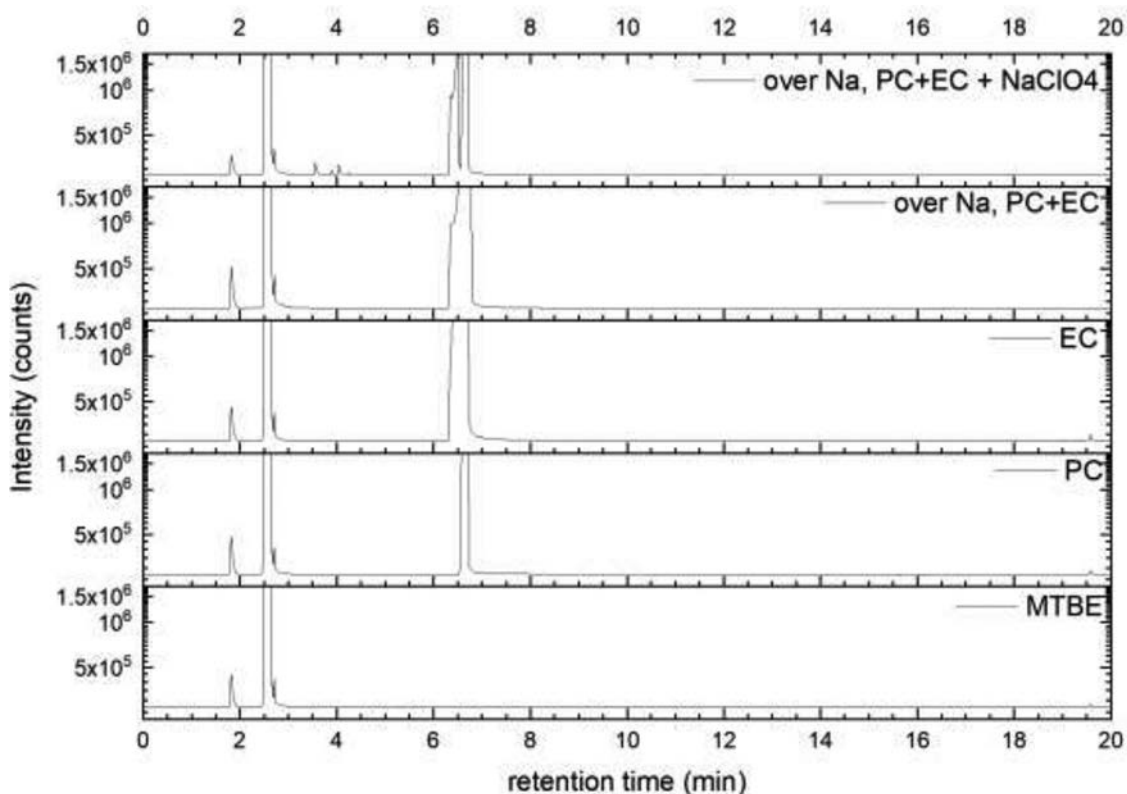
Fig. 4. Gas chromatogram of MTBE, PC, EC, PC+EC+Na without NaClO$_4$ and PC+EC+Na with NaClO$_4$ (detector: FID).
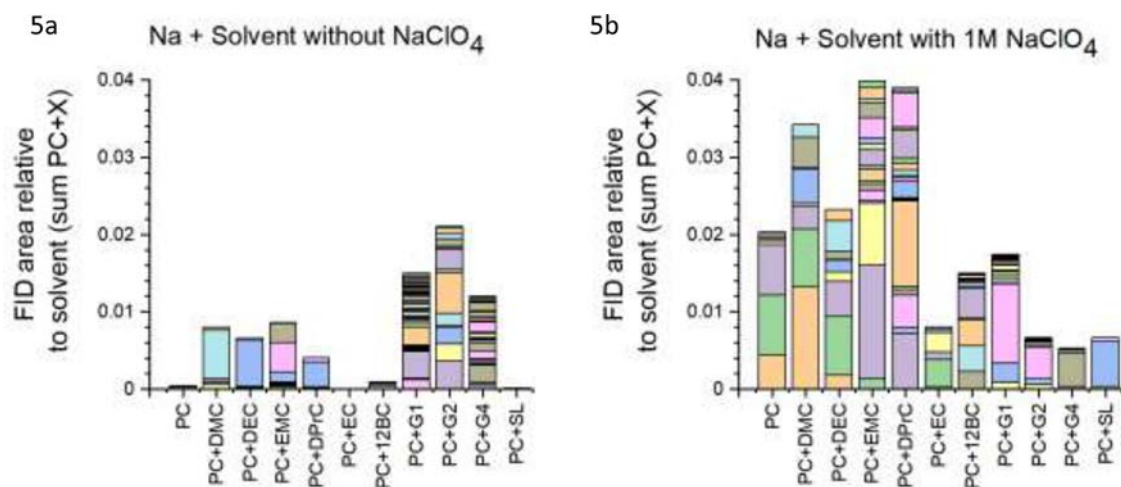

Fig. 5. Gas chromatography results of electrolytes with and without NaClO$_4$ salt including sodium metal after 4 months of storage. Same colors of the bars do not represent the same substances, each set of defragmentation products is individual for each mixture. All data are corrected regarding pure solvent impurities and impurities arising from the GC diluent MTBE. Decomposition of EMC to DMC and DEC is also neglected (see text).

fragments can be caused by characteristic fragments like, $[CO_2]^{\bullet+}$ ($m/z = 44$), $[H_3C\text{-}CH_2\text{-}O]^{\bullet+}$ ($m/z = 45$), $[CH_2\text{-}O\text{-}(CO)]^{\bullet+}$ ($m/z = 58$), $[H_3C\text{-}CH_2\text{-}CH_2\text{-}O]^{\bullet+}$ ($m/z = 59$), $[H_3C\text{-}O\text{-}(CO)]^{\bullet+}$ ($m/z = 59$), $[H_3C\text{-}CH_2\text{-}O\text{-}(CO)]^{\bullet+}$ ($m/z = 73$) $[H_3C\text{-}CH_2\text{-}CH_2\text{-}O\text{-}(CO)\text{-}O]^{\bullet+}$ ($m/z = 103$) and $[H_3C\text{-}O\text{-}(CO)\text{-}O\text{-}CH\text{-}CH_3]^{\bullet+}$ ($m/z = 103$), $[H_3C\text{-}CH_2\text{-}O\text{-}(CO)\text{-}O\text{-}CH_2]^{\bullet+}$ ($m/z = 103$), $[H_3C\text{-}CH_2\text{-}O\text{-}(CO)\text{-}O\text{-}CH_3]^{\bullet+}$ ($m/z = 104$). According to the general trend within a compound class interacting with the Optima 5MS capillary column, the dicarboxylates exhibit increasing retention times with larger alkyl chain length: 10.65 min (D) > 9.42 min (C) > 8.92 min (B) > 8.37 min (A). Compound C and compound D exhibit a good NIST match of

890/1000 (compound C) and 862/1000 (compound D) (EI fragmentation match), respectively as well as good accordance of the RI (C: found: 1340, NIST: 1348; compound D: found: 1517, NIST: 1537). Unfortunately, compounds A and B are not listed neither in the NIST nor in the Wiley database. A distinction between B1 and B2 was not possible within this study. Since the formation of the coupling products occurs independently of NaClO$_4$, it can be assumed that the interaction of the solvent molecules with the metal surface is most crucial. Other than described by Simone et al. for EC+DMC mixture containing NaPF$_6$, the kinetic of the decomposition of PC+DMC+1M NaClO$_4$ in the presence of sodium is sig-
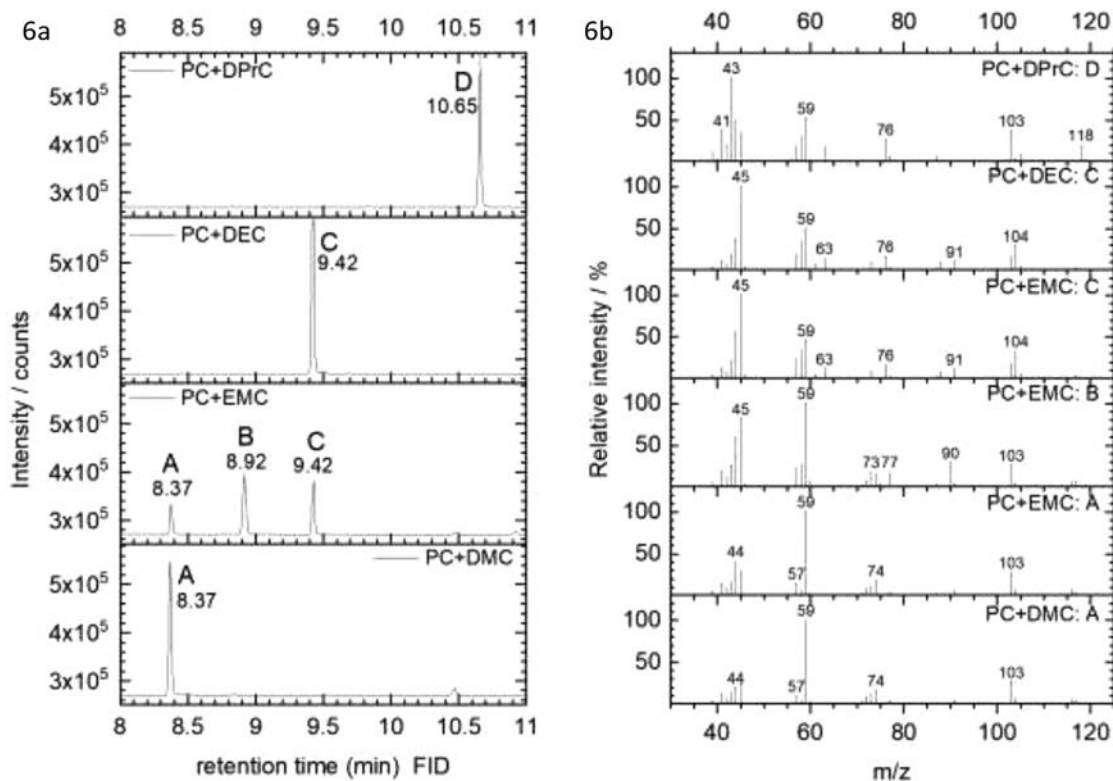
Fig.6. (6a) Chromatograms of mixtures of sodium and PC+linear carbonates (PC+DMC, PC+EMC, PC+DEC, PC+DPrC; without salt) detected by FID detector as well as (6b) the mass EI fragmentation from these peaks (detected from the mass spectrometer within the same analysis run).
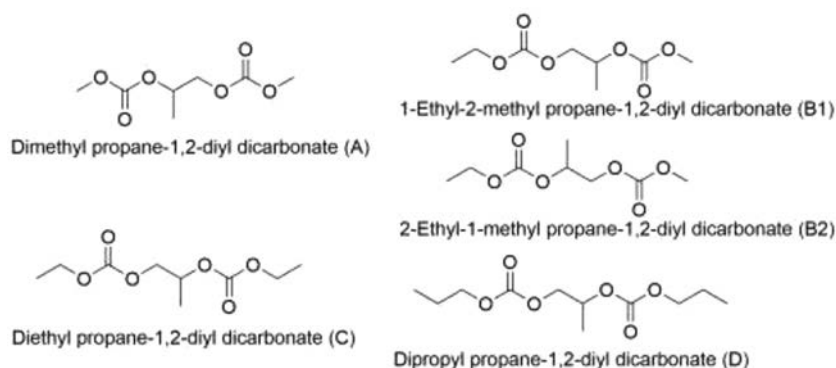

Fig. 7. Proposed structures based on NIST validation (match **C**: 890/1000; match **D**: 862/1000), reasonable retention times compared to dialkyl ethane-1,2-diyl dicarbonates and EI fragmentation. Compounds **A** and **B** are neither in NIST nor in Wiley database available.

nificantly lower, as can be seen from the relative intensities (Fig. DB-12) and which is supported from quantitative measurements (not shown) [43]. This indicates a reduced kinetic behavior in case of propylene carbonate compared to ethylene carbonate and might be due to the additional methyl group contributing to strong steric shielding. The formation of the di-carbonate coupling products is often described by a radical mechanism including alkoxide derivatives (methoxide, ethoxide) [49,43]. In this context it should be noted that ethanol was detected in the "PC+DEC+NaClO$_4$+Na" sample in small traces, but not in the "PC+DEC+Na" sample without NaClO$_4$, where also coupling product was also found.

It can be observed that a similar peak pattern as described for compounds A-D occurs between 10.4 min and 13.5 min in case of DMC, DEC, EMC as well as DPrC-containing mixtures. These peaks are mentioned as **?2, ?3, ?4** and **?5** in Table DB-8 (Data in Brief). Strong signals from mass fragmentation are observed at PC+DMC

(**?2**, $m/z = 117, 59, 73$), PC+EMC (**?4**, $m/z = 117, 59, 131$), PC+DEC (**?3**, $m/z = 103, 131, 59$) and PC+DPrC (**?5**, $m/z = 103, 44, 59$). Based on the fragmentation pattern described above, these fragments can be attributed to typical fragments which originate from carbonate containing compounds by EI fragmentation. However, a structure clarification (e.g. with two isopropyl groups as described by Takeda et al. [71] for EC/DEC electrolytes) was not possible within this study (GC-MS/EI analysis), but such coupling products seem to be very likely.

It was observed that the gas peak at the beginning of the chromatogram increases significantly for almost all electrolytes with NaClO$_4$ salt (Fig. DB-23, Data in Brief) after long-term storage (4 month). Based on a strong $m/z = 44$ signal this was attributed to CO$_2$ formation. However, such a behavior is not observed, when the mixture is stored shorter times (< 1 month). With the GC setup and the 5MS column it is not possible to separated CO$_2$ from the other gases (O$_2$, Ar, N$_2$), but the mass signal ($m/z = 44$) as well
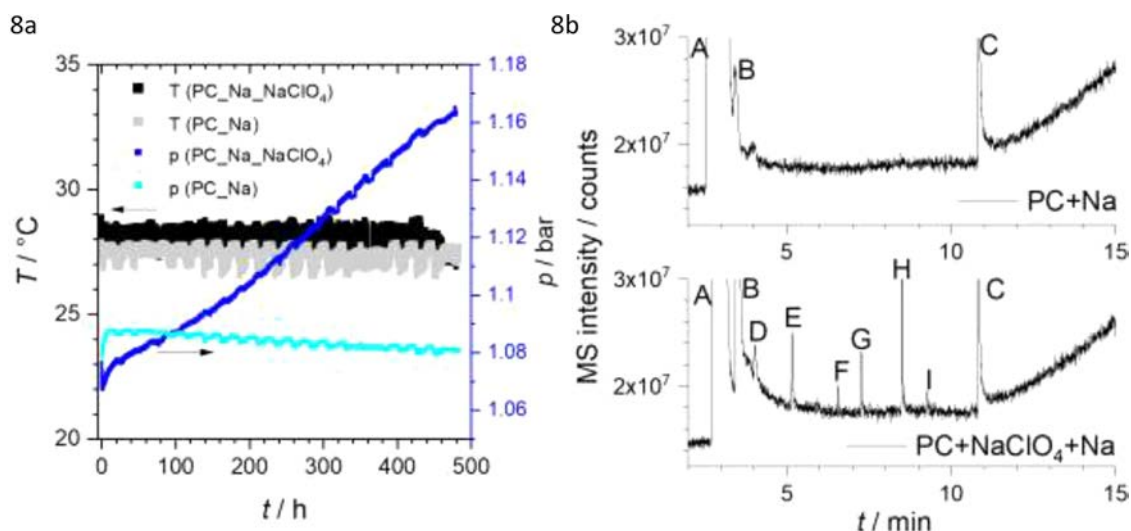
Fig. 8. 8a. Comparison of two electrolytes (PC, PC + NaClO$_4$) during storage over sodium metal. The cell pressure as well as the cell temperature is shown in dependence of the storage time. 8b. GCMS analysis of the gas phase from PC + 1 M NaClO$_4$ + Na metal and PC + Na metal. Assignment of compound, when possible (based on validation): A = gas peak (O$_2$/Ar/N$_2$/CO$_2$), B = propylene oxide (NIST, confirmed with pure compound), C = propylene carbonate (NIST, confirmed with pure compound), D = traces of MTBE, E = isopropyl acetate (NIST), F = Isopropyl methyl carbonate (NIST), G = isopropyl isobutyrate (NIST), H = diisopropyl carbonate (NIST, confirmed with pure compound), I = unknown (m/z = 41, 43, 57, 58, 102).
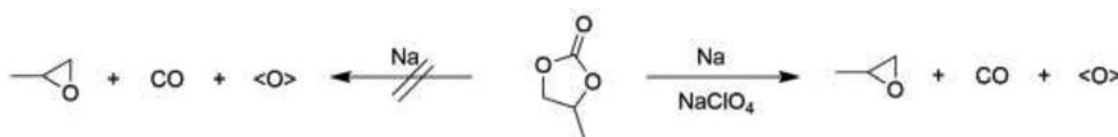

Fig. 9. Reaction pathway of the formation of CO and propylene oxide in the presence of NaClO$_4$ at room temperatures. A significant formation of O$_2$ was not found thus we balanced the equation by using <O>.

as its intensity compared to blank samples supports the interpretation as CO$_2$ formation.

To verify the gas evolution, a PAT-press-cell (EL-Cell) including a gas reservoir was used and a small vial with 0.6 ml electrolyte ("pure PC" or "PC+1 M NaClO$_4$") including sodium (several Na pieces were placed in the electrolyte) was set and observed regarding pressure and gas-formation qualitatively. Within 20 days, a pronounced increase of the internal pressure (approx. 100 mbar) was observed (Fig. 8a) for the "PC+NaClO$_4$"-electrolyte whereas "pure PC" shows no sign of gas evolution. The gas of both samples was taken after 20 days and injected into a GC device (Figs. 8b, DB-24, Data in Brief). In the gas of the sample "PC+NaClO$_4$+Na", following compounds were detected (with rough information about the signal intensity in the gas sample): H$_2$ (little), CO (strong), propylene oxide (strong), isopropyl acetate (little), isopropyl isobutyrate (little), di-(*iso*-propyl) carbonate (medium), propylene carbonate (medium) (two GC devices were used for the detection, one for gas determination with MS/WLD and one with MS/FID detection). In the sample "PC+Na" only following compounds could be detected: H$_2$ (little), propylene oxide (little), propylene carbonate (medium). In these samples, surprisingly no CO$_2$ was found (detection limit ~ 50 ppm). Since significant amounts of propylene oxide (retention time FID peak max: 2.12 min, RI = 489) are found in the GC measurements for almost all samples including NaClO$_4$ salt, this indicates that PC decomposes in the presence of NaClO$_4$ and Na (Fig. 9). In salt-free mixtures, such products were not detected or rather in small traces. While in the study of Pan et al. di-(*iso*-propyl) carbonate was also found [32], the formation of the described ether compound (OBHE, called "1,1-oxydi-bis(2-hydroxypropyl)ether" but the given structure indicates "1,1′-oxybis(propan-2-ol)" [32]) could not be confirmed in this study. However, the assigned compound isopropyl isobutyrate

exhibit similar mass fragmentation, namely m/z = 43, 71, 89, 59, 42. The gas analysis was done exemplarily for PC only, a systematic study of the gaseous products for all mixtures is indeed beyond the scope of the manuscript. Thus, it seems that CO$_2$ is formed only in the later stage of very long storage, and initially the formation of CO dominates.

It is known that additives (e.g. FEC, LiBOB at room temperature) can stabilize the surface of Na (forming a sufficient protection layer) in order to avoid the decomposition of the electrolyte. Shortly, these effects were observed clearly for the mixtures above. For this purpose, 3% FEC was added to individual NaClO$_4$ containing electrolytes (PC+DMC, PC+DEC, PC+G1) and storage was repeated over Na. Accordingly to literature results it was found that the mixtures containing FEC remained clear and showed no clouding or discoloration over a period of 8 weeks at room temperature [32,39,41]. A concentration series (PC+DMC+NaClO$_4$+FEC with FEC content between 0.1 and 3 wt.-%, stored over sodium metal) reveals that this electrolyte protection can be observed over a period of 15 days starting from low FEC concentrations ($\geq$ 0.25 wt.-%; 0.1 wt.-% FEC was not able to protect the Na/electrolyte completely). This finding indicates a FEC-stabilized surface that blocks the corresponding decomposition of the solvents. Correspondingly, no coupling products were found via GC-MS, when FEC is present in at least 0.25 wt.-% content.

New di-carbonate derivatives could be identified in the study and a basis for comparison with other groups is provided by mentioning retention index numbers. It was possible to consider the role of NaClO$_4$ in the formation of decomposition products. The GC analyses demonstrate that the use of Na as electrode material led to various gaseous and soluble side products which can affect the cell and the performance of any kind of half cells or other electrochemical set-ups. This aggravates the use of Na as counter elec-
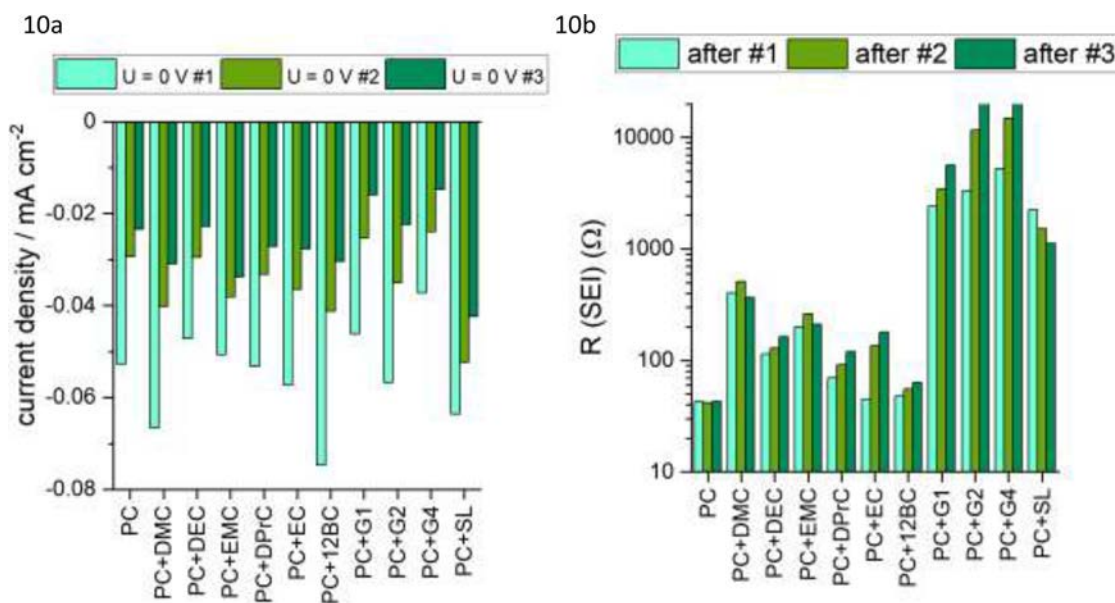
Fig. 10. (Fig. 10a) Cu-Na half cells. Current density at $U = 0$ V vs. Na/Na$^+$ as well as (Fig. 10b) the fitted circuit element R(SEI) from EIS spectra measured at $U = 0$ V vs. Na/Na$^+$ after every CV step ending from 2 V $\rightarrow$ 0 V at 2 mVs^{-1} (#1 = 3 V $\rightarrow$ 0 V; #2 = #1 $\rightarrow$ 2 V $\rightarrow$ 0 V; #3 = #2 $\rightarrow$2 V $\rightarrow$ 0 V).

trode and reference electrode significantly, especially when no additives are employed. The lowest formation of by-products was observed in PC and PC+EC electrolytes without NaClO$_4$, while PC+G4 and PC+SL in the presence of NaClO$_4$ were the mixtures where the minimum amounts of by-products were formed.

3.5. Electrochemical studies

All electrolyte mixtures were investigated in electrochemical experiments of the Na|Cu-cells. The cells were cathodically polarized between 2 V and 0 V vs. Na/Na$^+$ (same as below) for 3 cycles (marked as #1, #2 and #3 in Fig. 10a), followed by repeated cycling to more negative potential (-0.5 V) (marked as #4 and #5 in Fig. 10b). In this investigation, the intercalated anode materials were avoided to be used as the working electrode, to exclude the influence of charge carrier storage but to take a glance at the comparison of the interface layers formed through the reduction decomposition of various electrolyte components.

First, the influence of applying a voltage to Cu-Na half cells (2 V to 0 V to 2 V) was measured (Fig. 10a). The current response during the potential scan from 2 V to 0 V indicates the decomposition of the different liquid electrolytes, related to the interface layer formed at the copper side. It can be observed that the current density from 2 V to 0 V is consistently in a low range (mainly < 0.1 mA$\bullet$cm^{-2} range), but obviously dependent on the electrolyte component used. Especially, the current density at 0 V was also correlated to the reduction current caused by the interface layer formation reaction; the latter was usually considered to be a critical factor at the very first cell-cycling, influencing the SEI-layer formation and columbic efficiency. Moreover, within three cycles studied, the current density becomes even smaller, which is also an indication that no progressive reaction is taking place. That could be attributed to the isolated properties of the pre-formed interface layer, reducing the current densities at 0 V (#2 and #3) by shielding the electronic transfer at the Cu-electrode. This is indicative for an evaluation of the SEI forming ability at cell anode, to impede the electrolyte continuous decomposition during the cell cycling.

In parallel, the impedance at 0 V vs. Na/Na$^+$ was recorded, in each case after a short relaxation as soon as the voltage of 0 V was reached (Fig. 10b). Using the equivalent circuit model in Fig. 11, the
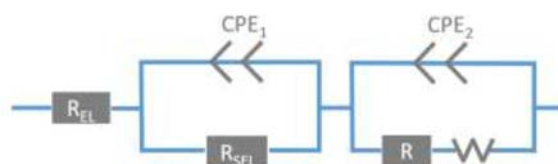

Fig. 11. Impedance model for data fitting procedure to obtain the R$_{SEI}$ resistance values.

impedance measurement was fitted and the SEI resistance (R_{SEI}) was determined. This reflects the resistance at the interfaces. It can be seen that in case of the glyme compounds very high resistances in the kΩ range are found, whereas in the case of the carbonate samples, resistances in the lower hundred-Ω range are obtained (Fig. 10b). This agrees well with the change in Na color in Section 3.3 (Tables 3 and DB-6, Data in Brief), which suggests a pronounced reaction on the Na surface in case of glyme components. Accordingly, it is suggested that the developing orange color on the Na metal surface in the case of the PC+glyme electrolytes is indication of a layer formation leading to a significant increase in resistance. Additionally, it is found that the SEI resistance in case of the glyme electrolytes increases over the cycle number continuously. This effect is less pronounced for the carbonate mixtures. This might specify a non-stable surface and an ongoing surface reaction as observed for the dark reddish-colored visual sample (Table 3). In other words, PC+glyme electrolytes strengthen the interface layer in terms of shielding ability of the SEI layer. Glymes might therefore be used to gradually adjust the SEI resistance when used in lower amounts (few%) even by a continuous surface reaction. PC+SL exhibits a decreasing number of R_{SEI} indicating a more stable surface layer.

Sodium deposition is not observed if the potential is decreased to 0 V vs. Na/Na$^+$. Therefore, plating-stripping experiments were performed by lowering the potential to -0.5 V vs. Na/Na$^+$ in Na-Cu cells. The results are shown in Fig. 12. It can be seen that strong plating and stripping effects of Na are observed for PC+EC and PC+DMC electrolyte, whereas almost no plating-stripping is seen for glyme-containing electrolytes. In this case the overpotential caused by the surface coating onto Na may be too large to see
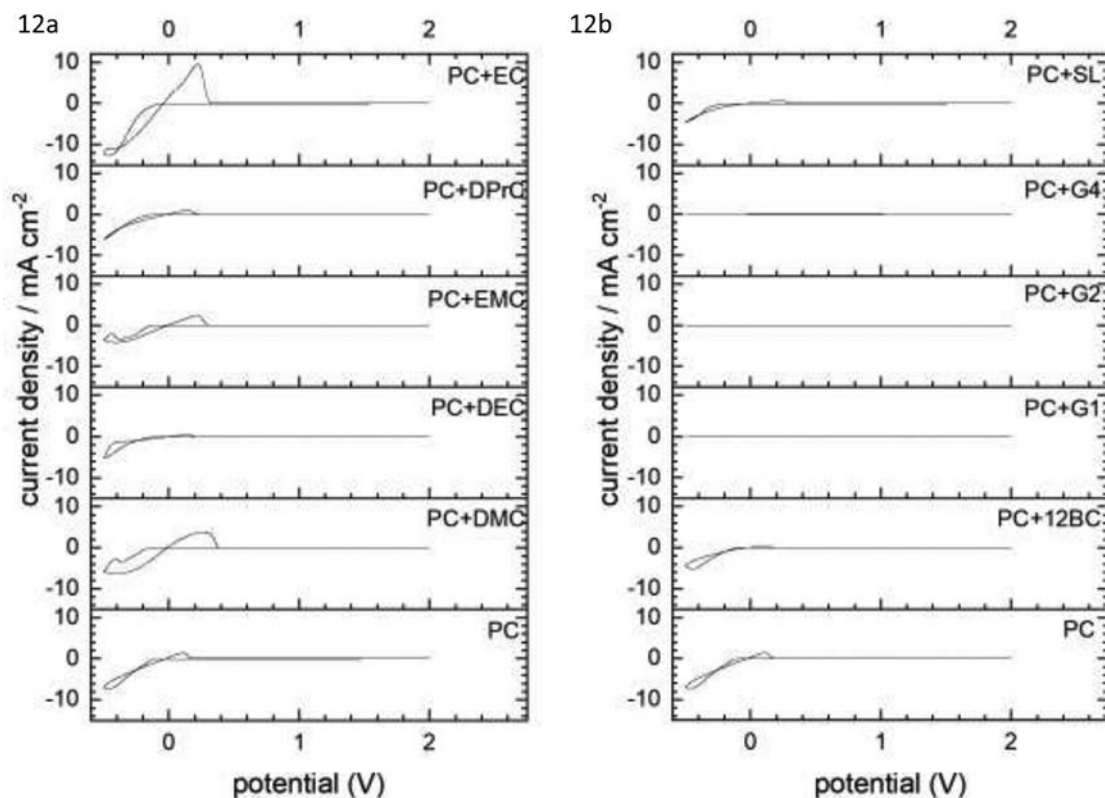
Fig. 12. Cu-Na half cells of 1 M NaClO$_4$ electrolytes with the composition mentioned were cycled between -0.5 V and 2.75 V vs. Na/Na$^+$.

Fig. 13. Images of Cu electrode and separators after dissembling the Cu/Na cells from plating-stripping experiments, exemplarily shown for "PC+1 M NaClO$_4$" and "PC+G2+1 M NaClO$_4$".

these effects (overpotential hampers Na to plate onto Cu). In all cases, the integral value of the Na plating step is much larger than that from the stripping step. This is caused by overpotential effects and irreversible reactions onto fresh Na surface. Less pronounced deposition of Na on Cu in the case of glyme-based electrolytes was also observed when the cells were opened. Much less Na on Cu was found than in the case of carbonate-based electrolytes.

Satisfactory agreement of the results are observed from the Cu electrodes and separators after disassembling of the coin cells. When high current densities occurred within the plating-stripping test, a clear appearance of Na layers and/or black precipitate was observed. Two samples are shown exemplarily, namely "PC+1 M NaClO$_4$" and "PC+G2+1 M NaClO$_4$" (Fig. 13). While the deposition of Na on Cu and in the separator can be clearly observed in PC and the other samples showing plating-stripping behavior, the Cu electrodes and separators in the glyme-based electrolytes are almost blank. This corresponds to the finding that plating simply does not yet occur in the glyme-based electrolytes, presumably due to the overvoltage caused by the inert layers that form.

Half-cell tests in Na - hard carbon configuration are often done to examine the performance and aging of electrolytes. As described above, the electrolyte will affect the cycling seriously in terms of forming decomposition products as it has been seen visually and in

GC measurements. For this reason, additives are commonly used to stabilize this interface, such as FEC. However, the addition of additives also changes the electrolyte properties, as mentioned, and accordingly the electrolyte can no longer be compared directly with the electrolyte investigated above. For this reason, we decided to investigate the performance of the electrolytes directly in full cells, namely in the configuration hard carbon versus sodium manganese oxide (NMO), to exclude metal-electrolyte reactions. In Fig. 14, results of the cycling are shown, specifically Fig. 14a for 125 cycles for longer-term stability and Fig. 14b for performance test.

In this context, electrolyte stability is tested up to 125 cycles for a qualitative statement only. A cell cycling for 250 cycles without a performance test is shown in Fig. DB-25 (Data in Brief) exemplarily for PC electrolyte. It can be observed that glyme-containing electrolytes exhibit the worst stability as well as the worst performance which is noteworthy as glyme based electrolytes are used for Na ion electrolytes widely. Even PC+G1 electrolyte exhibits poorer performance data if the current rate during discharge exceeds 2C than cyclic carbonate mixtures or PC+SL electrolyte. Nevertheless, all electrolytes show principally a relatively good retention of charge for 100 cycles (> 80%. See Fig. 14b).

In order to address the safety issues due to the NaClO$_4$ salt, a thermal gravimetric analysis (TGA) coupled with a differential
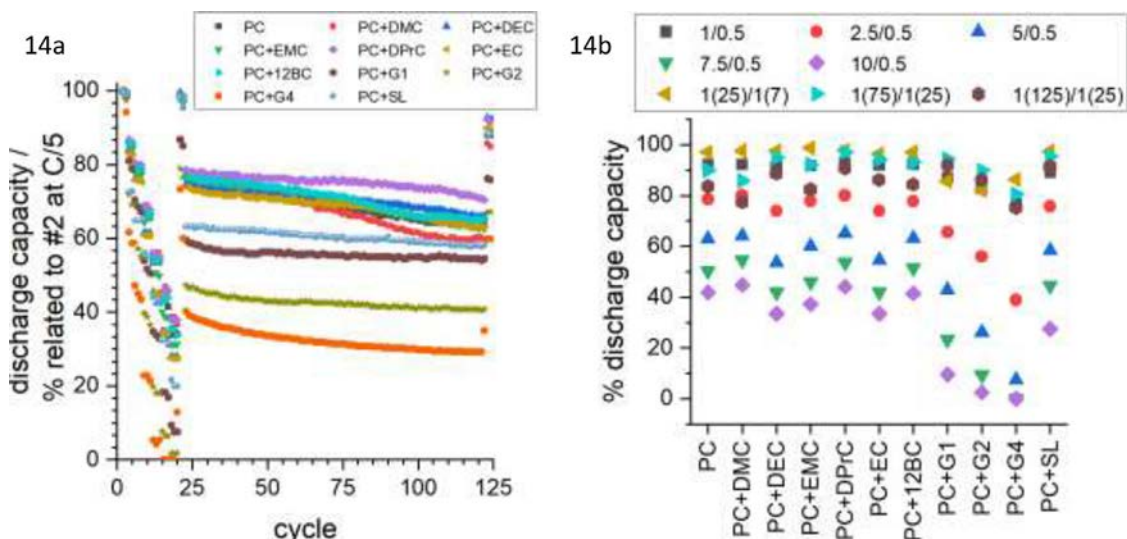
Fig. 14. Cycling data of NMO//HC full cells at room temperature (coin cells). Fig. 14a: Cycling within 125 cycles at various current rates is shown. All data are discharge capacities related to the second cycle which was done at 0.2 C discharge. The current rates are mentioned in the experimental section for detail. Charging was done at current rate of 0.5 C. Fig. 14b: Percentage of discharge capacity retention is depicted for selected current rates. In brackets cycle number is provides, e.g. 1(25) means: current rate of 1 in the 25th cycle.

scanning calorimetry (DSC) analysis was done for the PC+EC+1 M NaClO$_4$ electrolyte (Fig. DB-26, Data in Brief). As shown by Eshetu et al., pure NaClO$_4$ is stable up to > 500 °C without any mass loss [49]. Additionally it was claimed that PC+EC mixtures release lower rates of exothermic heat independently of the conducting salt than mixtures of cyclic and linear carbonates [49]. Consistently, the TGA-DSC results of the PC+EC+1 M NaClO$_4$ electrolyte confirms both findings that (1) exothermic reactions occur only above temperatures of 200 °C, after a strong endothermic peak, which is caused by the evaporation/boiling of EC and PC (mass loss of ~ 82%), and (2) the exothermic peak between 215 and 255 °C is of relative small intensity (-89.4 J•g^{-1}). DSC measurements, which were done by Ponrouch et al. of pure PC+1M NaClO$_4$ additionally confirms that such an electrolyte system is stable up to 350 °C [3].

3.8. Sustainability of the solvents

Table 5 presents the hazard level (HL) and hazard traffic light (HTL) for each of the individual precursor materials as there is no data available regarding the chemical behavior and consequent potential hazardousness of the electrolyte mixtures. No data available was found in the ECHA database for 1,2-butylene carbonate. The first two columns, NaClO$_4$ and PC, relate to the salt and solvent which are present in every mixture. The remaining columns relate to the additional solvent that distinguishes the mixtures from each other. For each hazard statement, the single HL is presented and the total HL is calculated as described in Eq. (1). The hazard levels for the glymes (mono-, di- and tetra-glyme) have been found among the largest values, with great contributions associated to health hazards such as germ cell mutagenicity, carcinogenicity and reproductive toxicity. The latter one is also critical for SL. The base compounds (NaClO$_4$ and PC) entail the lowest hazard levels among all the compounds. The G1 has the greatest amount of hazard statements, a total of 8, including a ´danger´ one and three EU harmonized statements. The DMC has the lowest HL, corresponding to only one hazard statement.

A *life cycle assessment* (LCA) analysis was performed to gain a deeper understanding of the impact of each mixture which had been defined with a 1:1 mol:mol ratio of PC and a second solvent (namely solvent B), with the addition of a NaClO$_4$ salt with a concentration of 1M. A base amount of electricity was considered

for the stirring process of the electrolytes, calculated taking into account the specific density of each mixture. The results in this section are presented for 1 L of electrolyte mixture for two impact categories given the perceived relevance of the related topics in the research community: ´climate change potential´ánd ´mineral resource scarcity´(Fig. 15). The results are expressed as kg of CO$_2$ and kg of copper equivalents, respectively. A detailed view of the remaining impact categories can be found in Table DB-9 (Data in Brief). Regarding ´climate change potential´, PC has been found to be the largest contributor in 10 out of 11 mixtures and the electrolyte based on PC carries the highest carbon footprint, a total of 4.8 kg CO$_2$-eq. The synthesis of PC requires propylene oxide as an input material, which has a more energy- and emission- intensive pre-chain in contrast to the other precursor materials.

The contributions of the NaClO$_4$ originate from the direct energy consumption during its synthesis and from the supply chain of sodium chlorate. The synthesis of DPrC and 12BC have also been found to entail significant CO$_2$-eq. emissions. Regarding resource scarcity, the electrolyte using PC only was found again to entail moderately larger impacts of about 1.8 kg Cu-eq. It was also found that the NaClO$_4$ salt significantly contributes to the total impacts of every mixture. This is due to the fact that the synthesis of the salt is normally performed by means of electrolysis with a platinum anode that is consumed in the process. Platinum has a high characterization factor within this category, thus leading to the observed high impacts. The pre-chain of propylene oxide for PC production also leads to relevant contributions within this category.

The first part of the assessment, related to the potential hazardousness of the compounds used in each mixture, suggests that a higher record of hazards does not necessarily lead to a higher hazard level. Compounds such as EMC or DPrC are presented with seven different hazard warnings, but the total hazard level is well below some others. For instance, G4 only has one hazard statement and yet its hazard level is significantly higher. This is because the specific hazard ´reproductive toxicity´is deemed as critical, with a LT value several orders of magnitude lower than most others. Most physical hazards relate to flammability but the scores for this statement are associated to high LT values in comparison to those allocated to some health hazards. In particular, the hazard statements ´germ cell mutagenicity´, ´carcinogenicity´and ´reproductive toxicity´entail the highest hazard levels, therefore,

Table 5
Hazard level (HL) and hazard traffic light (HTL) of the common solvent, common salt and additional solvent of each different mixtures including EU harmonized risk (labeled as "[H]"). No data available for 12BC. Colored cells: rot = danger, yellow = warning, green = not toxic, no classification or not tested.

		NaClO$_4$	PC	EC	DEC	DMC	EMC	DPrC	SL	G1	G2	G4
Reach registered		Y	Y	Y	Y	Y	N	N	Y	Y	Y	Y
Total HL (x 10^{-2})		5.5	4.0	14.5	5.02	0.02	8.02	8.02	22.0	45.02	20.02	20.0
HTL (all values given in x 10^{-2})												
Physical hazards	Explosive											
	Flammable				0.02	0.02[H]	0.02	0.02		0.02[H]	0.02[H]	
	Gas under pressure											
	Self-reactive											
	Pyrophoric											
	Self-heating											
	Water reactant											
	Oxidizing	2.0[H]										
	Corrosive to metals											
Health hazards	Acute toxicity[a] — o	1[H]		1			1	1	1[H]	1		
	d						1	1		1		
	i						1	1	1	1[H]		
	Irritant[b] — s		2	2	2		2	2		2		
	e	2	2[H]	10	2		2	2				
	Respiratory or skin sensitization											
	Germ cell mutagenicity									10		
	Carcinogenicity									10		
	Reproductive toxicity								20	20[H]	20[H]	20[H]
	Specific target organ toxicity exposure[c] — si			1	1		1	1				
	rp	0.5		0.5								
	Aspiration hazard											
Env.	Hazardous to the aquatic environment[d] — a											
	c											

[a] o = oral; d = dermal; I = inhalation. [b] s = skin; e = eye. [c] si = single; rp = repeated. [d] a = acut, c = chronic
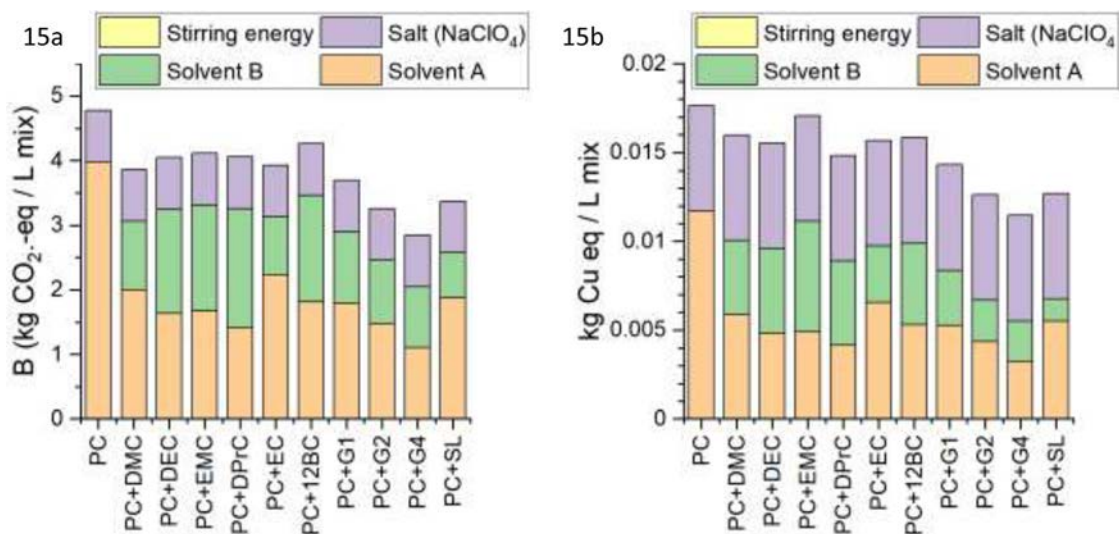

Fig. 15. LCA results for climate change (15a) and mineral resource scarcity (15b). The stirring energy is very small, thus this is almost not visible on the top of the bars.

compounds falling within those categories, as it is the case of the glymes, are perceived as potentially more hazardous.

Regarding the LCA, as seen in Fig. 15, the G4-containing electrolyte entails a more favorable environmental footprint, whereas the one using solely PC as solvent has in general the worst profile. This conclusion can also be extracted from the results presented in Table DB-9 when comparing the values in all different impact categories. In particular, the use of EMC is associated to toxicity issues and the use of DEC records the highest cumulative energy demand. In general, most contributions from each mixture result from the cumulated impacts of the pre-chain of the precursors and almost no individual hotspots have been identified. Special attention shall be given to the electrolyte mixture using SL. The synthesis of this compound involves consumption of sulfur dioxide, which is in itself but also from its manufacturing process a critical air pollutant and acidic agent. The results must be interpreted as indicative, given that in most cases several manufacturing routes exist for each precursor, meaning that a range of different environmental profiles could be obtained. In this study, the most common commercial routes as found in literature have been chosen to model the synthesis of precursor compounds, but in some cases, these correspond to outdated industrial processes that do not necessarily represent the current state-of-the art synthesis mechanisms.

The results presented are complementary between methodologies since they describe different sustainability aspects along the supply chain of each electrolyte mixture. On the one hand, the HTL and HL are related to potential risks arising from mishandling of different materials whereas the LCA relates to impacts generated along the life cycle of each product. For instance, the HTL and HL methodologies suggest that G4 is a potentially hazardous agent, but the LCA indicates a lower environmental footprint when this substance has been used. A combination of such methodologies is specially recommended when assessing the sustainability of products that are largely composed by chemical agents.

4. Conclusion

In this study, selected electrolytes are investigated, namely mixtures of PC, PC+DMC, PC+DEC, PC+EMC, PC+DPrC, PC+EC, PC+12BC, PC+monoglyme, PC+diglyme, PC+tetraglyme, and PC+SL including $NaClO_4$ as conducting salt in 1 M concentration for application in sodium-ion batteries. The solubility of $NaClO_4$ in all mixtures with exception of DPrC is sufficient for preparation of the electrolytes. It is revealed that calculations based on the AEM approach are able to achieve good agreement with experimental data in terms of density, conductivity and viscosity. The highest conductivity values at 25 °C are found for PC+G1 (10 mS•cm^{-1}) > PC+G2 (7.9 mS•cm^{-1}) > PC+DMC (7.4 mS•cm^{-1}) > PC+EC (7.1 mS•cm^{-1}) > others, while the lowest viscosity data are received for PC+G1(3.4 mPa•s) < PC+EMC (3.9 mPa•s) < PC+DMC = PC+DEC (4.1 mPa•s) < PC+G2 (4.3 mPa•s) < others. Temperature dependency of all electrolytes reveal an Arrhenius-like behavior with flow activation energies in the order of 11.1 kJ•mol^{-1} (PC+G1) - 23.1 kJ•mol^{-1} (PC+SL). It is unveiled that the reactivity of electrolyte regarding storage over Na metal depends severely on the presence of $NaClO_4$. High reactivity is seen in case of "PC+linear carbonates+$NaClO_4$" and "PC+glymes" (without $NaClO_4$). All glyme containing electrolytes show a visible color-change of the Na surface indicating a film formation onto the Na surface. The most optically stable electrolytes are both PC and PC+EC. In GCMS measurements decomposition products are detected and compared with a semi-quantitative approach. These measurements confirm the trend of less reactivity (storage over Na) in case of cyclic carbonates (PC, "PC+EC", "PC+12BC"), "PC+SL" as well as "PC+glymes+$NaClO_4$" and "PC+SL+$NaClO_4$". It is shown that linear (DMC, DEC, EMC, DPrC) and cyclic carbonates (PC) form

dialkane propane-1,2-diyl dicarbonate coupling products in the presence of Na independent from the conducting salt. In addition, coupling products of higher molecular masses were also detected. A clear difference in reactivity was observed in the analysis of gaseous products. Thus, it was found that significant amounts of gases formed in the presence of $NaClO_4$, namely CO and propylene oxide. In contrast, this reaction proceeds only very slowly or not at all without $NaClO_4$, since in this case CO was not detected and propylene oxide only in traces. No pressure increase was seen within 20 days of storage in this case. Electrochemical measurements expose that glyme containing electrolytes cause a film formation onto Na metal which can be seen from high contact resistances and suppression of stripping plating to -0.5 V va. Na/Na$^+$. Extensive plating-stripping is found for 1 M $NaClO_4$ electrolyte "PC+EC" (best) > "PC+DMC" > "PC" > "PC+other carbonates" ~ "PC+SL" ≫ PC+glymes. In spite of high conductivity values for glyme-containing PC electrolytes, the performance in NMO//HC cells was found to be inadequate, especially at current rates above 2C. An in-depth hazard analysis of the mixtures discloses that mixtures containing glyme compounds as well as sulfolane exhibit significantly higher toxicity, which can be seen on hazard levels (HL) of ≥ 0.02. Contrary, a life cycle assessment (LCA) analysis unfolds an almost balanced behavior of the electrolytes in terms of climate change potential and resources with minor favoring of the glyme based mixtures as well as PC+SL. The study supports the usage of PC+EC as a favorite electrolyte formulation, especially when Na metal is present.

Declaration of Competing Interest

The authors declare that they have no known competing financial interests or personal relationships that could have appeared to influence the work reported in this paper.

Credit authorship contribution statement

Andreas Hofmann: Conceptualization, Data curation, Investigation, Project administration, Supervision, Visualization, Validation, Writing – original draft, Writing – review & editing. **Zhengqi Wang:** Investigation, Visualization, Writing – review & editing. **Sebastian Pinto Bautista:** Investigation, Visualization, Writing – review & editing. **Marcel Weil:** Project administration, Supervision, Writing – review & editing. **Freya Müller:** Investigation, Writing – review & editing. **Robert Löwe:** Investigation, Writing – review & editing. **Luca Schneider:** Resources, Writing – review & editing. **Ijaz Ul Mohsin:** Resources, Writing – review & editing. **Thomas Hanemann:** Funding acquisition, Project administration, Resources, Supervision, Writing – review & editing.

Acknowledgments

References

[1] J.Y. Hwang, S.T. Myung, Y.K. Sun, Sodium ion batteries: present and future, Chem. Soc. Rev. 46 (2017) 3529.
[2] R. Dugas, A. Ponrouch, G. Gachot, R. David, M.R. Palacin, J.M. Tarascon, Na reactivity toward carbonate-based electrolytes: the effect of FEC as additive, J. Electrochem. Soc. 163 (2016) A2333.

[3] A. Ponrouch, E. Marchante, M. Courty, J.M. Tarascon, M.R. Palacín, In search of an optimized electrolyte for Na ion batteries, Energy Environ. Sci. 5 (2012) 8572.

[4] D. Monti, E. Jonsson, A. Boschin, M.R. Palacin, A. Ponrouch, P. Johansson, Towards standard electrolytes for sodium ion batteries: physical properties, ion solvation and ion-pairing in alkyl carbonate solvents, Phys. Chem. Chem. Phys. 22 (2020) 22768.

[5] T.D. Vo, H.V. Nguyen, Q.D. Nguyen, Q. Phung, V.M. Tran, P.L.M. Le, Carbonate solvents and ionic liquid mixtures as an electrolyte to improve cell safety in sodium ion batteries, J. Chem. 2019 (2019) 1.

[6] C.Y. Li, J. Patra, C.H. Yang, C.M. Tseng, S.B. Majumder, Q.F. Dong, J.K. Chang, Electrolyte optimization for enhancing electrochemical performance of antimony sulfide/graphene anodes for sodium ion batteries–carbonate-based and ionic liquid electrolytes, ACS Sustain. Chem. Eng. 5 (2017) 8269.

[7] Y. Lee, J. Lee, H. Kim, K. Kang, N.S. Choi, Highly stable linear carbonate-containing electrolytes with fluoroethylene carbonate for high-performance cathodes in sodium-ion batteries, J. Power Sources 320 (2016) 49.

[8] J.Y. Jang, H. Kim, Y. Lee, K.T. Lee, K. Kang, N.S. Choi, Cyclic carbonate based–electrolytes enhancing the electrochemical performance of $Na_4Fe_3(PO_4)_2(P_2O_7)$ cathodes for sodium ion batteries, Electrochem. Commun. 44 (2014) 74.

[9] A.M. Skundin, T.L. Kulova, A.B. Yaroslavtsev, Sodium ion batteries (a review), Russ. J. Electrochem. 54 (2018) 113.

[10] N. Tapia-Ruiz, A.R. Armstrong, H. Alptekin, M.A. Amores, H. Au, J. Barker, R. Boston, W.R. Brant, J.M. Brittain, Y. Chen, M. Chhowalla, Y.S. Choi, S.I.R. Costa, M. Crespo Ribadeneyra, S.A. Cussen, E.J. Cussen, W.I.F. David, A.V. Desai, S.A.M. Dickson, E.I. Eweka, J.D. Forero-Saboya, C.P. Grey, J.M. Griffin, P. Gross, X. Hua, J.T.S. Irvine, P. Johansson, M.O. Jones, M. Karlsmo, E. Kendrick, E. Kim, O.V. Kolosov, Z. Li, S.F.L. Mertens, R. Mogensen, L. Monconduit, R.E. Morris, A.J. Naylor, S. Nikman, C.A. O'Keefe, D.M.C. Ould, R.G. Palgrave, P. Poizot, A. Ponrouch, S. Renault, E.M. Reynolds, A. Rudola, R. Sayers, D.O. Scanlon, S. Sen, V.R. Seymour, B. Silván, M.T. Sougrati, L. Stievano, G.S. Stone, C.I. Thomas, M.M. Titirici, J. Tong, T.J. Wood, D.S. Wright, R. Younesi, roadmap for sodium-ion batteries, J. Phys. Energy 3 (2021) 031503.

[11] J. Song, B. Xiao, Y. Lin, K. Xu, X. Li, Interphases in sodium ion batteries, Adv. Energy Mater. 8 (2018) 1703082.

[12] G.G. Eshetu, T. Diemant, M. Hekmatfar, S. Grugeon, R.J. Behm, S. Laruelle, M. Armand, S. Passerini, Impact of the electrolyte salt anion on the solid electrolyte interphase formation in sodium ion batteries, Nano Energy 55 (2019) 327.

[13] E. Wang, Y. Niu, Y.X. Yin, Y.G. Guo, Manipulating electrode/electrolyte interphases of sodium ion batteries: strategies and perspectives, ACS Mater. Lett. 3 (2020) 18.

[14] M. Mandl, J. Becerer, D. Kramer, R. Mönig, T. Diemant, R.J. Behm, M. Hahn, O. Böse, M.A. Danzer, Sodium metal anodes: deposition and dissolution behaviour and SEI formation, Electrochim. Acta 354 (2020) 136698.

[15] J. Fondard, E. Irisarri, C. Courrèges, M.R. Palacin, A. Ponrouch, R. Dedryvère, SEI composition on hard carbon in Na ion batteries after long cycling: influence of salts (NaPF6, NaTFSI) and additives (FEC, DMCF), J. Electrochem. Soc. 167 (2020) 070526.

[16] R. Mogensen, D. Brandell, R. Younesi, Solubility of the solid electrolyte interphase (SEI) in sodium ion batteries, ACS Energy Lett. 1 (2016) 1173.

[17] Q. Pan, D. Gong, Y. Tang, Recent progress and perspective on electrolytes for sodium/potassium-based devices, Energy Storage Mater. 31 (2020) 328.

[18] M. Li, C. Wang, Z. Chen, K. Xu, J. Lu, New concepts in electrolytes, Chem. Rev. 120 (2020) 6783.

[19] A. Mauger, C. Julien, A. Paolella, M. Armand, K. Zaghib, Recent progress on organic electrodes materials for rechargeable batteries and supercapacitors, Materials 12 (2019) 1770.

[20] Q. Li, J. Chen, L. Fan, X. Kong, Y. Lu, Progress in electrolytes for rechargeable Li based batteries and beyond, Green Energy Environ. 1 (2016) 18.

[21] R. Mogensen, S. Colbin, R. Younesi, An attempt to formulate non-carbonate electrolytes for sodium ion batteries, Batter. Supercaps 4 (2021) 791.

[22] T. Chen, J. Guo, Y. Zhuo, H. Hu, W. Liu, F. Liu, P. Liu, J. Yan, K. Liu, An inactive metal supported oxide cathode material with high rate capability for sodium ion batteries, Energy Storage Mater. 20 (2019) 263.

[23] A. Darwiche, L. Bodenes, L. Madec, L. Monconduit, H. Martinez, Impact of the salts and solvents on the SEI formation in Sb/Na batteries: an XPS analysis, Electrochim. Acta 207 (2016) 284.

[24] E. Flores, G. Åvall, S. Jeschke, P. Johansson, Solvation structure in dilute to highly concentrated electrolytes for lithium ion and sodium ion batteries, Electrochim. Acta 233 (2017) 134.

[25] I.D. Gocheva, M. Nishijima, T. Doi, S. Okada, J.I. Yamaki, T. Nishida, Mechanochemical synthesis of NaMF3 (M=Fe, Mn, Ni) and their electrochemical properties as positive electrode materials for sodium batteries, J. Power Sources 187 (2009) 247.

[26] S. Komaba, T. Ishikawa, N. Yabuuchi, W. Murata, A. Ito, Y. Ohsawa, Fluorinated ethylene carbonate as electrolyte additive for rechargeable Na batteries, ACS Appl. Mater. Interfaces 3 (2011) 4165.

[27] A. Ponrouch, R. Dedryvère, D. Monti, A.E. Demet, J.M. Ateba Mba, L. Croguennec, C. Masquelier, P. Johansson, M.R. Palacín, Towards high energy density sodium ion batteries through electrolyte optimization, Energy Environ. Sci. 6 (2013) 2361.

[28] N. Recham, J.N. Chotard, L. Dupont, K. Djellab, M. Armand, J.M. Tarascon, Ionothermal synthesis of sodium based fluorophosphate cathode materials, J. Electrochem. Soc. 156 (2009) A993.

[29] R. Ruffo, R. Fathi, D.J. Kim, Y.H. Jung, C.M. Mari, D.K. Kim, Impedance analysis of $Na_{0.44}MnO_2$ positive electrode for reversible sodium batteries in organic electrolyte, Electrochim. Acta 108 (2013) 575.

[30] N. Yabuuchi, M. Kajiyama, J. Iwatate, H. Nishikawa, S. Hitomi, R. Okuyama, R. Usui, Y. Yamada, S. Komaba, P2-type Nax[Fe$_{1/2}$Mn$_{1/2}$]O$_2$ made from earth-abundant elements for rechargeable Na batteries, Nat. Mater. 11 (2012) 512.

[31] G. Yan, D. Alves-Dalla-Corte, W. Yin, N. Madern, G. Gachot, J.M. Tarascon, Assessment of the electrochemical stability of carbonate-based electrolytes in Na ion batteries, J. Electrochem. Soc. 165 (2018) A1222.

[32] K. Pan, H. Lu, F. Zhong, X. Ai, H. Yang, Y. Cao, Understanding the electrochemical compatibility and reaction mechanism on Na metal and hard carbon anodes of PC-based electrolytes for sodium ion batteries, ACS Appl. Mater. Interfaces 10 (2018) 39651.

[33] C. Cao, H. Wang, W. Liu, X. Liao, L. Li, Nafion membranes as electrolyte and separator for sodium ion battery, Int. J. Hydrog. Energy 39 (2014) 16110.

[34] K. Du, C. Wang, L.U. Subasinghe, S.R. Gajjela, M. Law, A. Rudola, P. Balaya, A comprehensive study on the electrolyte, anode and cathode for developing commercial type non-flammable sodium-ion battery, Energy Storage Mater. 29 (2020) 287.

[35] P. Moreau, D. Guyomard, J. Gaubicher, F. Boucher, Structure and stability of sodium intercalated phases in olivine FePO$_4$, Chem. Mater. 22 (2010) 4126.

[36] L. Othman, K.B.M. Isa, W.G. Chong, N.H. Zainol, S.M. Samin, Z. Osman, R. Yahya, Ionic conductivity, morphology and transference number of sodium ion in PMMA based gel polymer electrolytes, Key Eng. Mater. 594-595 (2013) 696.

[37] A. Ponrouch, A.R. Goñi, M.R. Palacín, High capacity hard carbon anodes for sodium ion batteries in additive free electrolyte, Electrochem. Commun. 27 (2013) 85.

[38] K. Subramanyan, Y.S. Lee, V. Aravindan, Impact of carbonate-based electrolytes on the electrochemical activity of carbon-coated Na$_3$V$_2$(PO$_4$)$_3$ cathode in full-cell assembly with hard carbon anode, J. Colloid Interface Sci. 582 (2021) 51.

[39] Y. Rangom, R.R. Gaddam, T.T. Duignan, X.S. Zhao, Improvement of hard carbon electrode performance by manipulating SEI formation at high charging rates, ACS Appl. Mater. Interfaces 11 (2019) 34796.

[40] M. Benchakar, R. Naéjus, C. Damas, J. Santos-Peña, Exploring the use of EMImFSI ionic liquid as additive or co-solvent for room temperature sodium ion battery electrolytes, Electrochim. Acta 330 (2020) 135193.

[41] K. Pfeifer, S. Arnold, J. Becherer, C. Das, J. Maibach, H. Ehrenberg, S. Dsoke, Can metallic sodium electrodes affect the electrochemistry of sodium ion batteries? Reactivity issues and perspectives, Chem. Sustain. Chem. 12 (2019) 1.

[42] A. Bouibes, N. Takenaka, T. Fujie, K. Kubota, S. Komaba, M. Nagaoka, Concentration effect of fluoroethylene carbonate on the formation of solid electrolyte interphase layer in sodium ion batteries, ACS Appl. Mater. Interfaces 10 (2018) 28525.

[43] V. Simone, L. Lecarme, L. Simonin, S. Martinet, Identification and quantification of the main electrolyte decomposition by-product in Na ion batteries through FEC: towards an improvement of safety and lifetime, J. Electrochem. Soc. 164 (2016) A145.

[44] M.J. Piernas-Muñoz, E. Castillo-Martínez, J.L. Gómez-Cámer, T. Rojo, Optimizing the electrolyte and binder composition for sodium prussian blue, Na1-x Fex+(1/3) (CN)6 •yH$_2$O, as cathode in sodium ion batteries, Electrochim. Acta 200 (2016) 123.

[45] J. Shi, L. Ding, Y. Wan, L. Mi, L. Chen, D. Yang, Y. Hu, W. Chen, Achieving long–cycling sodium ion full cells in ether-based electrolyte with vinylene carbonate additive, J. Energy Chem. 57 (2021) 650.

[46] S. Komaba, W. Murata, T. Ishikawa, N. Yabuuchi, T. Ozeki, T. Nakayama, A. Ogata, K. Gotoh, K. Fujiwara, Electrochemical Na insertion and solid electrolyte interphase for hard-carbon electrodes and application to Na ion batteries, Adv. Funct. Mater. 21 (2011) 3859.

[47] U. Purushotham, N. Takenaka, M. Nagaoka, Additive effect of fluoroethylene and difluoroethylene carbonates for the solid electrolyte interphase film formation in sodium ion batteries: a quantum chemical study, RSC Adv. 6 (2016) 65232.

[48] A. Bhide, J. Hofmann, A.K. Durr, J. Janek, P. Adelhelm, Electrochemical stability of non-aqueous electrolytes for sodium ion batteries and their compatibility with Na(0.7)CoO$_2$, Phys. Chem. Chem. Phys. 16 (2014) 1987.

[49] G.G. Eshetu, S. Grugeon, H. Kim, S. Jeong, L. Wu, G. Gachot, S. Laruelle, M. Armand, S. Passerini, Comprehensive insights on the reactivity of electrolytes based on sodium ions, Chem. Sustain. Chem. 9 (2016) 462.

[50] D. Reber, R. Figi, R.S. Kühnel, C. Battaglia, Stability of aqueous electrolytes based on LiFSI and NaFSI, Electrochim. Acta 321 (2019) 134644.

[51] R. Stockhausen, A. Hofmann, L. Gehrlein, T. Bergfeldt, M. Müller, H. Ehrenberg, A. Smith, Quantifying absolute amounts of electrolyte components in lithium ion cells using HPLC, J. Electrochem. Soc. 168 (2021) 080504.

[52] E.R. Logan, E.M. Tonita, K.L. Gering, J.R. Dahn, A critical evaluation of the advanced electrolyte model, J. Electrochem. Soc. 165 (2018) A3350.

[53] K.L. Gering, Prediction of electrolyte conductivity: results from a generalized molecular model based on ion solvation and a chemical physics framework, Electrochim. Acta 225 (2017) 175.

[54] K.L. Gering, Prediction of electrolyte viscosity for aqueous and non-aqueous systems: results from a molecular model based on ion solvation and a chemical physics framework, Electrochim. Acta 51 (2006) 3125.

[55] G. Rodriguez-Garcia, J. Braun, J. Peters, M. Weil, Hazard statements: looking for alternatives to toxicity evaluation using LCA, Mater. Tech. 105 (2018) 517.

[56] Regulation (EC) No 1272/2008 of the European parliament and of the council, Off. J. Eur. Union L353 (2008).

[57] H. Stahl, D. Bauknecht, A. Hermann, W. Jenseit, A.R. Köhler, C. Merz, M. Möller, D. Schüler, M. Vogel, L. Jörissen, U. Storr, Ableitung von Recyclingund Umweltanforderungen und Strategien zur Vermeidung von Versorgungsrisiken bei innovativen Energiespeichern, Umweltbundesamt, 2016.

[58] Directive 2012/18/EU, Official Journal of the European Union, L 197 (2012) 1.

[59] ISO, ISO 14040Environmental Management: Life Cycle Assessment – Principles and Framework, British Standards Institution, 2006.

[60] ISO, ISO 14044Environmental Management: Life Cycle Assessment – Requirements and Guidelines, British Standards Institution, 2006.

[61] M.A.J. Huijbregts, Z.J.N. Steinmann, P.M.F. Elshout, G. Stam, F. Verones, M. Vieira, M. Zijp, A. Hollander, R. van Zelm, ReCiPe2016: a harmonised life cycle impact assessment method at midpoint and endpoint level, Int. J. Life Cycle Assess. 22 (2016) 138.

[62] Z. Zhang, X. Ma, J. Zhang, F. He, S. Wang, Effect of crystal structure of copper species on the rate and selectivity in oxidative carbonylation of ethanol for diethyl carbonate synthesis, J. Mol. Catal. A Chem. 227 (2005) 141.

[63] Z.L. Shen, X.Z. Jiang, W.J. Zhao, A new catalytic transesterification for the synthesisof ethyl methyl carbonate, Catal. Lett. 91 (2003) 63.

[64] Y. Li, Y. Zhang, B. Xue, Y. Guo, Synthesis of dipropyl carbonate by transesterification over KNO3/MCM-48, J. Mol. Catal. A Chem. 287 (2008) 9.

[65] Shell Oil Company, Process for the preparation of propylene carbonate, United States Patent, US7728164B2 (2010).

[66] Texaco Chemical Company, Process for preparing alkylene carbonates, United States Patent, US5003084A (1971).

[67] Phillips Petroleum Company, Production of sulfolane, United States Patent, US3622598A (1971).

[68] Ferro Corporation, Method of producing glycol ethers, United States Patent, US20040044253A1 (2004).

[69] E. Kováts, Gaschromatographische Charakterisierung organischer Verbindungen. Teil 1: retentionsindices aliphatischer Halogenide, Alkohole, Aldehyde und Ketone, Helv. Chim. Acta 41 (1958) 1915.

[70] H. Van den Dool, P.D. Kratz, A generalization of the retention index system including linear temperature programmed gas-liquid partition chromatography, J. Chromatogr. 11 (1963) 463.

[71] S. Takeda, W. Morimura, Y.H. Liu, T. Sakai, Y. Saito, Identification and formation mechanism of individual degradation products in lithium-ion batteries studied by liquid chromatography/electrospray ionization mass spectrometry and atmospheric solid analysis probe mass spectrometry, Rapid Commun. Mass Spectrom. 30 (2016) 1754.

[72] T. Sasaki, T. Abe, Y. Iriyama, M. Inaba, Z. Ogumi, Suppression of an alkyl dicarbonate formation in Li ion cells, J. Electrochem. Soc. 152 (2005) A2046.

[73] H. Yoshida, T. Fukunaga, T. Hazama, M. Terasaki, M. Mizutani, M. Yamachi, Degradation mechanism of alkyl carbonate solvents used in lithium-ion cells during initial charging, J. Power Sources 68 (1997) 311.

[74] M.W. Grützke, W. Weber, W. Martin, N. Sascha, Structure determination of organic aging products in lithium ion battery electrolytes with gas chromatography chemical ionization mass spectrometry (GC-CI-MS)†, RSC Adv. 6 (2016) 57253.

[75] T. Sasaki, T. Abe, Y. Iriyama, M. Inaba, Z. Ogumi, Formation mechanism of alkyl dicarbonates in Li ion cells, J. Power Sources 150 (2005) 208.

[76] H. Kim, S. Grugeon, G. Gachot, M. Armand, L. Sannier, S. Laruelle, Ethylene bis-carbonates as telltales of SEI and electrolyte health, role of carbonate type and new additives, Electrochim. Acta 136 (2014) 157.

Repository KITopen

Dies ist ein Postprint/begutachtetes Manuskript.